Impact of a new radiation package, McRad, in the ECMWF Integrated Forecasting System

January 11, 2008

J.-J. Morcrette[a1], H.W. Barker[b], J.N.S. Cole[c], M.J. Iacono[d],

R. Pincus[e]

[a]ECMWF, Shinfield Park, Reading, RG2 9AX, United Kingdom

[b] Environment Canada, Toronto, ON, Canada

[c] Dept. Earth and Ocean Sciences, Univ. British Columbia, Vancouver, BC, Canada

[d] Atmospheric and Environmental Research, Inc., Lexington, MA, USA

[e] CIRES, Univ. Colorado/NOAA Earth Systems Research Laboratory, Physical Science Division, Boulder, CO, USA

[1]Corresponding author: Jean-Jacques Morcrette, email: Morcrette@ecmwf.int

ABSTRACT

A new radiation package (McRad) has become operational with cycle 32R2 of the Integrated Forecasting System (IFS) of the European Centre for Medium-Range Weather Forecasts (ECMWF). McRad includes an improved description of the land surface albedo from MODIS observations, the Monte-Carlo Independent Column Approximation treatment of the radiation transfer in clouds, and the Rapid Radiation Transfer Model short-wave scheme.

The impact of McRad on year-long simulations at $T_L159L91$ and higher-resolution ten-day forecasts is then documented. McRad is shown to benefit the representation of most parameters over both short and longer time-scales, relative to the previous operational version of the RT schemes. At all resolutions, McRad improves the representation of the cloud-radiation interactions, particularly in the tropical regions, with improved temperature and wind objective scores through a reduction of some systematic errors in the position of tropical convection, due to change in the overall distribution of diabatic heating over the vertical, inducing a geographical redistribution of the centres of convection. While smaller, the improvement is also seen in the r.m.s. error of geopotential in the Northern and Southern hemispheres and over Europe.

Given the importance of the cloudiness in modulating the radiative fluxes, the sensitivity of the model to cloud overlap assumption (COA) is also addressed, with emphasis on the flexibility inherent to this new RT approach when dealing with COA.

The sensitivity of the forecasts to the space interpolation required to deal efficiently with the high computational cost of the RT parametrization is also revisited. A reduction of the radiation grid for the EPS (Ensemble Prediction System) is shown to be of little impact on the scores while reducing the computational cost of the radiation computations.

McRad is also shown to decrease the cold bias in ocean surface temperature in climate integrations with a coupled ocean system.

1. Introduction

While it had always been recognized that an accurate representation of the radiation transfer is a precondition for a good climate simulation, a similar requirement for weather forecasts was thought, in the 70s, to be a luxury, given the long time scale generally ascribed to radiative processes at the time. Table 1 gives the timeline of the major changes affecting the representation of the radiation transfer in the ECMWF model over the last twenty years. ECMWF, with its ten-day forecasts, was from its inception, one of the very first weather forecast centres where emphasis was put on having a reasonably accurate radiation transfer (RT) parametrization, interactive with humidity and cloudiness (Geleyn, 1977; Geleyn and Hollingsworth, 1979).

Even if by today's standards, these first versions of the ECMWF radiation codes were not free from systematic errors, they already provided interactivity with the temperature, water vapour and then a few years later with the distribution of the fractional cover and optical thickness of clouds provided by the diagnostic cloud scheme (Slingo, 1987). These first versions served their purpose with a fair description of the Equator-Pole gradient in the deposition of radiative energy and of the vertical distribution of the total radiative heating.

At the end of the '80s, the Intercomparison of Radiation Codes for Climate Models (ICRCCM, Fouquart et al., 1991) was the first opportunity to compare, in a systematic way results of GCM-type radiation schemes with line-by-line (LbL) models of the infrared radiation transfer and to document their successes and failures. A more extensive description of the characteristics of the early ECMWF schemes can be found in Morcrette (1991) together with a description of the RT schemes, originally developed at the University of Lille, which replaced these early schemes in May 1989. This replacement followed an assessment of the systematic errors in the forecast model linked to the representation of the radiative processes provided by these early schemes

(Morcrette, 1990). In the following years, cloud optical properties were revised following the availability of new parametrizations (Morcrette, 1993).

At the end of the '90s, following developments in line-by-line RT models and the emergence of much more accurate measurements of the surface radiation fields and of the temperature and water vapour profiles (mainly as part of the Atmospheric Radiation Measurement program of the U.S. Department of Energy, ARM, but also of dedicated surface radiation network: SURFRAD in the U.S.A., Baseline Surface Radiation Network, BSRN), it became possible to validate the clear sky radiation fields computed by a GCM-type RT scheme to within a few Wm^{-2} in the long-wave and to within 10-15 Wm^{-2} in the short-wave part of the spectrum.

In 2000, RRTM, the long-wave RT scheme (Mlawer et al., 1997) developed at AER, Inc., from the LBLRTM (line-by-line RT model: Clough et al., 1992; Clough and Iacono, 1995) was adapted to the ECMWF computer environment, extensively tested (Morcrette et al., 1998) and adopted as the operational long-wave RT scheme (Morcrette et al., 2001). In parallel, following comparisons with some of the surface observations discussed above (Morcrette, 2002a, 2002b), revisions were made to the short-wave radiation scheme (extended from 2 to 4 spectral intervals in June 2000, then to 6 spectral intervals in April 2002).

Despite the improvements brought to the representation of the clear sky radiative fluxes by these revised/new schemes, the handling of cloudiness had kept following an approach originally introduced twenty years earlier by Geleyn and Hollingsworth (1979). Various sensitivity studies (e.g., Morcrette and Fouquart, 1986; Barker et al., 1999; Morcrette and Jakob, 2000) had shown the huge impact that a change in cloud overlap assumption (COA) usually brings to the instantaneous radiative fluxes at the boundaries of the atmosphere and radiative heating rate profiles. Also, ground-based cloud radar measurements at a mid-latitude location (Hogan and Illingworth, 2000, 2003) were showing that the maximum-random COA generally used in

GCM-type RT schemes (Barker et al., 2003a) did not provide enough decorrelation even for cloud layers distributed continuously over the vertical (i.e., the observed cloud layers appear more randomly distributed on the vertical than model cloud layers distributed according to the maximum-random overlap). Such measurements, repeated at other locations as part of the ARM program, confirmed these early conclusions.

Unfortunately, the GCM-type RT schemes prevalent at the time could not easily be made flexible enough to accommodate such observationally-based cloud overlap distributions. This deficiency, together with concern about fisrt, the role of the spatial inhomogeneity in the distribution of the condensed water within a layer (first addressed by Cahalan et al., 1994, then by a number of authors among them Barker et al., 1999, Barker et al., 2003a, 2003b), and second, the upgrading of the gaseous absorption coefficients following the release of a new version of the spectroscopic database, were the background for the adoption of a new approach to radiation transfer.

This paper documents the various elements included in the new radiation package used in all configurations of the ECMWF IFS. Also McRad will be the radiation scheme used in a future reanalysis. Consequently, this paper is aiming at documenting its main impact on the various configurations of the model.

2. Description of a new radiation package for the ECMWF Integrated Forecast System

As part of the modifications to create the model library that became operational on 5 June 2007 (the so-called cycle 32 release 2, CY32R2), the radiation transfer package was modified along

three lines:

- the spectrally flat land surface albedo derived from ERBE (Earth Radiation Budget Experiment) satellite measurements was replaced by a land surface albedo with four components derived from MODIS (Moderate Resolution Imaging Spectroradiometer) satellite measurements: albedo for direct and diffuse radiation given for the two spectral intervals on both sides of 0.7 μm;

- the radiation transfer in clouds is treated following the Monte-Carlo Independent Column Approximation (McICA);

- the short-wave radiation scheme is based on the Rapid Radiation Transfer Model (RRTM), originally developed by Clough et al. (2005), making it fully consistent with the RRTM long-wave code, operational at ECMWF since June 2000.

In the following, this new radiation package is referred to as McRad. The resolution of the simulations and forecasts with the ECMWF IFS is given for example by $T_L159L91$, indicating a truncature retaining 159 spectral coefficients for the dynamics, a linear grid for the physics with 160 latitudes and up to 320 longitudes, and 91 levels on the vertical.

a. A climatology of land surface albedo derived from MODIS observations

A new climatology of land surface albedo has been introduced in the IFS to be used as boundary conditions in short-wave flux computations. Apart from being derived from more recent and more spatially detailed satellite observations than the previously operational land surface albedo derived from ERBE observations (Sellers et al., 1996), this MODIS albedo will be consistent with the MODIS-derived surface reflectances that will be used when computing synthetic

MODIS radiances for aerosol analysis as part of the GEMS-AERosol (Global Earth Monitoring using Satellite and in-situ data).

This new climatology was derived from the 2001-2004 datasets produced by Boston University (Schaaf et al, 2002), with processing over 16 day periods of the 1km spatial resolution MODIS observations. The wide-band albedo, given for direct and diffuse radiation in both the UV-visible and near-infrared parts of the short-wave spectrum replaces the monthly mean spectrally flat albedo previously derived from ERBE observations. Figure 1 presents for the month of April the UV-visible (0.3-0.7 μm), near-infrared (0.7-5.0 μm) components of the short-wave albedo derived from MODIS. Figure 2 compares the previous operational spectrally flat (0.3-5.0 μm) land surface albedo derived from ERBE observations with the equivalent surface albedo obtained from the ratio of the upward over downward short-wave fluxes computed with the new albedo.

Sets of 13-month long integrations at $T_L159L91$ were conducted with the two different representations of land surface albedo and the two radiation configurations (pre-McRad and McRad) within cycle 32R2 of the operational library. As seen in Table 2, the impact of the change from ERBE-derived to MODIS-derived land surface albedo on the climate of the IFS $T_L159L91$ model is small, whatever the radiation configuration. With the previous radiation configuration, the change of land surface albedo was somewhat detrimental, whereas with the McICA-based radiation, the change of land surface albedo brings some small improvements to the representation of the climate. Despite what could be thought as some sizeable changes in local albedo features (e.g., a general increase of about 0.05 over Sahara, a decrease of up to 0.10 over South of Central Russia), the impact in 10-day forecasts at $T_L399L62$ from the change in surface albedo is marginal. Figure 3 compares for the model with ERBE and MODIS albedos the parameter the most sensitive to this albedo change (mean error in temperature at 850 hPa).

With the pre-32R2 radiation package, the difference remains within 0.02 K after 10 days; it is slightly bigger (up to 0.08 K after ten days in the Northern hemisphere) with the McRad radiation package. Such differences are very small, and do not translate to any sizeable change in other parameters. Similar results are found for the $T_L799L91$ model configuration.

b. What is McICA?

At the grid-scale of a large-scale atmospheric model (LSAM), domain-averaged radiative fluxes in clouds with substantial horizontal and vertical variability can in principle be determined quite accurately using the plane-parallel independent column approximation (ICA) by averaging the flux computed for each class of cloud in turn (Cahalan et al., 1994; Barker et al., 1999). This approach neglects true three-dimensional effects, but those are generally minor (Barker et al., 2003a). Unfortunately, such an ICA-based method is too computationally expensive for dealing with radiation transfer (RT) in a LSAM. Various approximations have been introduced over the years to compute domain-averaged radiative fluxes for internally variable clouds, all invoking assumptions about the nature of the horizontal variability (e.g., Stephens, 1988; Oreopoulos and Barker, 1999; Cairns et al., 2000) or how cloud layers are linked over the vertical (Geleyn and Hollingsworth, 1979; Morcrette and Jakob, 2000; Li, 2002). Regardless of what assumptions are made about these unresolved structures, estimates of radiative heating should theoretically become increasingly unbiased at increasingly large spatial and temporal scales. However, this is generally not the case, and climate simulations have been shown to be very sensitive to seemingly small, but systematic, alterations to cloud optical properties (e.g., Senior, 1999).

Recently, Barker et al. (2002) and Pincus et al. (2003) introduced a new method for computing broadband radiative fluxes in LSAMs yielding unbiased radiative fluxes over an ensemble

average of one-dimensional RT simulations. It is referred to as the Monte-Carlo Independent Column Approximation (McICA). The most attractive features of McICA are two-fold: first, it extricates the description of the sub-grid scale cloud structure from the radiative transfer algorithm through a cloud generator that provides the cloud parameters for the radiation schemes by sampling the cloud information randomly from the cloud fraction and water profiles provided by the LSAM; second, its radiative fluxes, unbiased with respect to ICA, are consistent with assumptions made about the unresolved structure in other parts of the model (for example, the overlap assumption implicit in the calculations of precipitation from cloud layers and evaporation in the non-cloudy parts of underlying layers (Jakob and Klein, 1999)). In practice, this sub-grid scale cloud structure is related either to the overlapping of the cloud layers in the vertical and/or to the horizontal variability of the cloud characteristics. Whether in the vertical or in the horizontal, the cloud characteristics referred to above correspond to input parameters in a traditional radiation transfer scheme, namely the distribution of condensed water in various phases, that of the particle effective dimension, which together with the distribution of intervening gases should define the radiation exchange on the vertical within a grid of the LSAM. As ICA, McICA does not account for true three-dimensional transfer effects, but those can generally be neglected as shown by Räisänen et al. (2003) using fields produced every three hours over a day by a cloud-resolving-model (CRM) embedded in a LSAM.

The McICA approach is an approximation to the full Independent Column Approximation (ICA). As discussed by Barker et al. (2002) and Pincus et al. (2003), for the full ICA, the average monochromatic radiative flux, over a domain sub-divided in N columns, in which each layer can only have a cloud fraction of 0 or 1, is

$$\langle F \rangle = \frac{1}{N} \sum_{n=1}^{N} F_n \tag{1}$$

In sub-column n, using a radiation parametrization (plane-parallel, and considering a homogeneous cloud water distribution in all overcast layers) with a correlated k-distribution (CKD) approach (Lacis and Oinas, 1991) to deal with absorption, the total flux F_n is

$$F_n = \sum_{k=1}^{K} c_k F_{n,k} \tag{2}$$

where the summation is over the K absorption coefficients and c_k is the corresponding width of the part of the spectrum corresponding to the absorption coefficient k (spectral sub-interval k) in the correlated k-distribution.

Combining (1) and (2) gives

$$\langle F \rangle = \frac{1}{N} \sum_{n=1}^{N} \sum_{k=1}^{K} c_k F_{n,k} \tag{3}$$

A radiation code explicitly integrating the double sum in (3) would be far too expensive for GCM applications. The McICA solution to this problem is to approximate (3) as

$$\langle F \rangle_M = \sum_{k=1}^{K} c_k F_{n_k,k} \tag{4}$$

where $F_{n_k,k}$ is the monochromatic radiative flux in spectral sub-interval k with a randomly selected vertical cloud distribution n_k. From this definition, the McICA solution (4) equals the ICA solution only when all N sub-columns are identical or $N = 1$. As discussed in Räisänen and Barker (2004), McICA's incomplete pairing of sub-columns and spectral intervals ensures that its solution will contain random, but unbiased, errors.

McICA can in principle be used within any radiation transfer scheme provided the following conditions: 1/ a cloud generator is used to define how the cloud information is distributed over

each spectral element in the radiation spectrum and 2/ enough g-points (or spectral intervals) are available to make the profiles of cloud fraction and cloud water resulting from the summation over the whole distribution consistent with the original profiles. The application of the McICA approach involves using a cloud generator together with slightly modified but otherwise standard radiation schemes. A description of the radiation transfer schemes and of the cloud generator used in this study is given below.

c. Practical implementation of McICA in the ECMWF model

Table 3 summarizes the main features of the radiation package used in the operational model since 5 June 2007. The radiation fluxes are computed using the Rapid Radiation Transfer Models (RRTM), both in the long-wave and short-wave parts of the spectrum.

The ECMWF version of $RRTM_{LW}$ (Mlawer et al., 1997, Morcrette et al., 2001) describes the long-wave spectrum with 16 spectral intervals, corresponding to a total of 140 g-points (K_{LW} = 140 in Eqn 4). $RRTM_{SW}$ (Clough et al., 2005) describes the short-wave spectrum with 14 spectral intervals, corresponding to a total of 112 g-points (K_{SW} =112 in Eqn 4). Each of the 16/14 spectral intervals might have a different number of g-points (in the cumulative probability space directly derived from the correlated-k distribution), depending how much the absorption coefficient varies within the spectral interval, but also how much the spectral interval contributes overall to the total flux, and this over the whole depth of the atmosphere represented by the atmospheric model.

For each of these g-points, an essentially monochromatic type radiation transfer is carried out using a two-stream method with approximation of long-wave (LW) scattering and using a Delta two-stream method with scattering in the short-wave (SW). For liquid water clouds, the ef-

fective droplet radius is diagnosed from the cloud liquid water content following Martin et al. (1994); the effective ice particle size is diagnosed from the cloud ice water content following a modification of Ou and Liou (1995) in the reference scheme, and following Sun (2001) in the McRad scheme.

The McICA versions of $RRTM_{LW}$ and $RRTM_{SW}$ differ from the above versions in two respects: i/ Avoiding any explicit reference to cloud fraction greatly simplifies the parts of the algorithms devoted to the vertical integration, which now deal simply with optical thicknesses. For a given g-point, a cloud when present fully occupies a model layer. Therefore any cloudy calculation only involves modifying the optical parameters (optical thickness τ, single scattering albedo ω, and asymmetry factor g). ii/ This allows the removal of the 0.7 factor multiplying the cloud optical thickness, which had been introduced in 1997 (Cahalan et al., 1994; Tiedkte, 1996) in the ECMWF Integrated Forecasting System (IFS) to account approximately for the effect of cloud inhomogeneities at the sub-grid level.

As stated in Section 2.b, the McICA representation of cloud-radiation interactions requires the cloud information to be distributed by a cloud generator over the vertical with the constraint that the total cloudiness and cloud water loading for a grid-point is strictly conserved for an infinite number of draws of the cloud generator (and conserved to a high degree of approximation for a large number of draws as with 140 in the LW and 112 in the SW)

The purpose of the cloud generator is, starting from a cloud profile (cloud fraction and cloud water content) provided by a traditional cloud scheme (e.g., Tiedtke, 1993), to distribute randomly the cloud information (in terms of presence (1) or absence (0)) into each of the layers covered by the original cloud profile. This distribution is done N times (McICA with N going to infinity would be equal to ICA) with the constraint that a summation over the N profiles would recreate the original vertical distribution of partial cloudiness. In the ECMWF model, for each

radiation time-step (every one hour of model time for the $T_L799L91$ forecast) and each radiation grid-point, the cloud generator is used twice, to produce two cloud distributions relevant, respectively, to the 140 g-points of the LW- and 112 g-points of SW radiation schemes. We use the cloud generator of Räisänen et al. (2004), which vertically can distribute either the cloud cover according to a maximum-random overlap assumption (Morcrette and Jakob, 2000) or both the cloud cover and cloud water assuming a generalized overlap (Hogan and Illingworth, 2000, 2003).

Clouds when present occupy the full horizontal extent of the layer, and the vertical distribution of such clouds (of 0 or 1 cloud cover) is defined independently for each of the 140 (112) g-points of the long-wave (short-wave) scheme by the cloud generator, with the constraint that the total cloudiness and cloud water loading for a grid-point is conserved when N tends to infinity.

Most of the McRad results presented hereafter correspond to a generalized overlap with decorrelation lengths of 2 km for cloud cover and 1 km for cloud water, and a standard deviation of the cloud condensate normalized by the mean cloud condensate ($\frac{\sigma_l}{l}$) of 1. Only in section 3.d, will results corresponding to a generalized overlap with different decorrelation lengths, or to maximum-random overlap of the cloud layers be discussed. In all comparisons discussed hereafter, the pre-McRad model (CY31R2 operational model, hereafter referred to as OPE) uses the ECMWF six spectral interval version of the short-wave radiation code of Fouquart and Bonnel (1980), with a slightly different set of cloud optical properties marked by a cross (+) in Table 3. In tests not discussed here, it was shown that replacing the operational short-wave radiation scheme by $RRTM_{SW}$ alone or changing the cloud optical properties, while affecting the radiation fields, did not affect much the systematic errors shown by the ECMWF IFS in 13-month simulations at $T_L159L91$. Only the full McRad package with the suppression of the 0.7 inhomogeneity factor, the use of the McICA approach within $RRTM_{LW}$ and $RRTM_{SW}$, and the

revised cloud optical properties shows the positive impact discussed below.

d. A different radiation grid for McRad

Following a study of the dependence of radiation fields and model climate on (temporal and) spatial characteristics of the radiative forcing (Morcrette, 2000), a new interface for radiation computations was developed and implemented in October 2003. Radiation calculations are performed on a grid with a coarser resolution than the current model grid. Interpolation between model and radiation grids are performed using interfaces existing within the IFS libraries and this, as a result, helps reduce code maintenance. This radiation grid had been used since October 2003, with a coarsening factor of two in both latitude and longitude w.r.t. the rest of the model (e.g., the operational forecast model at $T_L 799$ is run with a radiation grid R399).

The introduction of McRad in the ECMWF IFS brought a sizeable increase in the computer time required for carrying out a given forecast. It must be stressed that this increase is not related to the McICA approach, as the McICA versions of $RRTM_{LW}$ and $RRTM_{SW}$ are slightly faster than the original versions as they are not dealing with fractional cloudiness, but just optical thicknesses, whether originating from clear-sky absorbers and aerosols, or the same plus cloud optical thickness. The increase is mainly linked to the use of $RRTM_{SW}$ with its 112 g-point radiative transfer computations compared with computations over the six spectral intervals of the previously operational SW scheme (Fouquart and Bonnel, 1980; Morcrette, 2002a).

The implementation of the more computer-intensive McRad has therefore led to the search for an optimal radiation grid for the different weather forecasting applications run at ECMWF. Table 4 presents for the various model configurations used at ECMWF an overview of the timing with and without McRad. Depending on the model resolution, associated time-step, and

the frequency for calling the full radiation schemes, the cost of the model integration increased from 15 to 29 percent. However, comparisons of results with the different radiation grids (from R399 to R95 for the $T_L799L91$ high-resolution model, from R255 to R31 for the $T_L399L62$ model run in the Ensemble Prediction System, from R159 to R31 for the $T_L159L91$ model used for seasonal forecasts) were systematically carried out.

For the choice of the radiation grid, a compromise has to be made between the computer time required to run a given configuration and how detailed one wants the representation of the spatial cloud structure and of its associated radiative fluxes to be. Different meteorological applications lead to different answers: For the high-resolution deterministic forecast where the position of clouds as affected by land-sea temperature and orographic effects is an important information, the highest radiation resolution is to be kept as much as possible. However, it must be kept in mind that McICA allows sub-grid scale information on the horizontal distribution of cloud elements to be taken into account (via the normalized standard deviation), so what appears as a reduced radiation grid in fact includes more information than the original radiation grid used with the pre-McRad scheme. For the Ensemble Prediction System (EPS), the constraint to have the highest radiation resolution possible can certainly be released (see section 4.b). A best compromise was chosen (R319 for T_L799, R95 for T_L399, $R63$ for T_L159), which allows the maximum benefit of McRad within the time constraints for delivering the various operational products. The coarsening of the radiation grid was shown to be of very little impact on the objective scores provided by higher-resolution models, which are discussed in section 4.

3. Results for seasonal simulations at $T_L159L91$

Two sets of annual simulations with either McRad or the operational radiation package have been carried out over the 13-month period between August 2000 and September 2001. Each set includes an ensemble of three simulations starting from analysed initial conditions 24-hours apart. Output parameters averaged over each ensemble and the September'00-August'01 period are presented as maps in Figs. 4 to 8. Global mean values for an extended list of parameters are given in Table 5, averaged over the year, and over the DJF and JJA three-month periods.

a. Radiative fields at the top of the atmosphere

McRad improves the behaviour of the model in a number of aspects: a change in the balance between long-wave and short-wave radiation heating leads to a noticeable shift in the location of the tropical cloudiness. This shift is particularly striking when comparing the model long-wave cloud forcing (LWCF: Fig. 4) and short-wave cloud forcing (SWCF: Fig. 5) with corresponding parameters from CERES observations. This is mainly a feature of McICA, as preliminary tests using $RRTM_{SW}$ (without the McICA approach) instead of the operational short-wave radiation code, or with a different set of cloud optical properties, changed somewhat the overall radiation budget at the top of the atmosphere, but without affecting the negative bias linked to too small a cloudiness over South America, Africa and the Tropical West Pacific. McRad improves markedly on the TOA radiation biases over these areas. As seen in Table 5, differences with CERES observations are improved with the new model, with a reduction of the global annual mean bias from -8.1 to -3.2 $W\ m^{-2}$ for OLR, from -10.0 to -5.8 $W\ m^{-2}$ for ASW, from -9.6 to -4.0 $W\ m^{-2}$ for LWCF, and from -5.2 to -0.2 $W\ m^{-2}$ for SWCF. More importantly, the reduction in biases is accompanied by reduction in standard deviations showing that temporally

(based on monthly averages) and spatially the location of the minima and maxima of the various fields are improved by McRad. Table 4 confirms that these improvements happen over the whole year, with a general improvement on the TOA radiative parameters also appearing for winter (DJF) and summer (JJA) conditions.

From Table 5 and the related figures, it is evident that the overall climate of the model is improved in terms of TOA radiation budget.

With McRad, the surface SW radiation is increased, a worse agreement with the Da Silva climatology (Da Silva and Levitus, 1994; over oceans only). However, for the ECMWF model run with an interactive ocean, the better geographical distribution of SW surface fluxes produced by the new radiation package has been found to be beneficial to the forecasts of ocean surface temperature (see section 3.e). A significant improvement is also seen in terms of temperature and humidity when compared to ERA40 analysis (Uppala et al., 2005).

b. Hydrological budget

As seen also in Table 5, the overall climate of the model is also improved in terms of the global water vapour (TCWV: total column water vapour) and cloud water distribution (TCLW: total column liquid water), and level of total precipitation (TP, compared in Table 5 to GPCP and SSM/I estimates). The only degradation is seen in surface SW radiation, which shows the annual mean difference to the Da Silva-Levitus climatology (over oceans only) roughly doubled. This is directly partly linked to slightly more transparent clouds induced by the McICA approach, but mostly to the transfer of convective cloudiness from tropical oceanic to tropical continental areas.

Despite the increase in surface SW radiation over the tropical oceans, it was found that for the

ECMWF model including an interactive ocean, the better geographical distribution of surface fluxes linked to the shift of the convection produced by McRad is beneficial to the forecasts of ocean surface temperature (see section 3.e).

Figure 6 presents the total precipitation and its comparison with GPCP observations. The improvements are less marked than for radiation fields. However a reduction of the deficit of precipitation over South America and Africa and a slight reduction of the overestimation of precipitation over the Pacific, Atlantic and Indian oceans are present, confirmed by the better global results, on an annual or seasonal basis, seen for total precipitation in Table 5, whether compared globally to GPCP or over the tropical ocean to SSM/I.

c. Temperature, humidity and wind errors

Figures 7 and 8 respectively present the zonal mean differences of temperature and humidity (Fig. 7) and zonal wind and vertical velocity (Fig. 8) averaged over the year. The McRad package improves on the temperature differences (Fig. 7 top) to ERA40 analyses, showing an overall warming of the troposphere, and a cooling of the stratosphere. This translates into a slight improvement in the zonal mean humidity w.r.t. ERA40 (Fig. 7 bottom). The impact on zonal mean zonal wind (Fig. 8 top) is somewhat smaller but generally positive. Impact on vertical velocity (Fig. 8 bottom) is mainly seen in the tropical area with a slight decrease in both the negative and positive difference to ERA40 between 30^oN and 30^oS. The differences to ERA40 of the annual mean of the wind at 200, 700 and 925 hPa (Fig. 9) show that McRad has a beneficial impact at all heights with a decrease of the errors over the tropical oceans. Particularly noticeable is the joint decrease of the mean wind error over the equatorial Indian ocean and Central North equatorial Pacific both at 925 and 200 hPa, the signal over the Pacific

consistent with an improvement of the Ferrel circulation.

d. Sensitivity to cloud overlap assumption

As already indicated in section 2.c, the use of a cloud generator external to the LW and SW radiation schemes to deal with the vertical overlap of clouds layers and potential inhomogeneity in the horizontal distribution of cloud water content makes easy the testing of various configurations. Sets of seasonal simulations were carried out in the same conditions as those discussed in the previous sections, with the McRad model configuration and different assumptions for the cloud vertical overlap and horizontal distribution of cloud water. As can be seen from Fig. 10, the impact on temperature of various decorrelation lengths for cloud cover (DLCC) or cloud water (DLCW), or switching to a maximum-random cloud overlap with provision for inhomogeneous cloud water distribution is much smaller than the impact of introducing the new radiation package. As can be seen from Table 6, each of these configurations is slightly different in terms of impact on radiation and other physical fields, and the configuration chosen for operational implementation in cycle 32R2 is the one which gives the best overall comparisons to observations.

e. Impact on climate integrations with a coupled ocean system

As part of the testing of the McRad package, sets of simulation with the model including a coupled ocean were run over ten years starting on 1 November 1994. One of the effects of McRad, namely the increase in downward solar radiation at the surface, is seen to improve the simulation of the ocean temperature particularly during the first two years of the simulations. Figure 11 presents for these two years the difference of the ocean annual mean temperature with

ERA40 for both versions of the model, and between themselves.

Over most of the tropical region, the bias in SST is decreased between 0.3 and 0.9 K, with a complex pattern of improvement. For example, over the northern parts of the Pacific and Atlantic oceans, McRad decreases the cold bias in SST, and decreases the warm bias over the Pacific tropical area and Southern region.

4. Impact on operational weather forecasts

a. High-resolution deterministic 10-day forecasts at $T_L799L91$

An experimental suite, parallel to the operational suite at $T_L799L91$ was run from July 2006 to April 2007. It included McRad and a series of data assimilation modifications, unlikely to affect the radiative fluxes beyond the first few hours in the forecasts. In the following, results are presented for the period December 2006-April 2007, with more specific diagnostics for January 2007. It must be stressed that the model response at T_L799 is similar to what was shown in section 3 for seasonal simulations. Here the emphasis is put on the short term response (12 hours to 10 days) of the model and on objective scores. The main impact of McRad, compared to the previously operational radiation scheme, is to modify separately the vertical distributions of the additional long-wave and short-wave heating induced by the presence of the clouds. This is linked first to the McICA approach, which replaces the previous 0.7 inhomogeneity factor scaling all cloud optical thicknesses in the long-wave and short-wave parts of the spectrum in the previous version of the radiation schemes, and second, to a lesser degree, to the revised cloud optical properties, particularly for ice clouds where the effective particle size is now diagnosed from temperature and the local ice water content (only temperature with the operational

configuration).

For clouds with the same profiles of cloud fraction and optical thickness, the McICA approach lets more short-wave radiation reach the surface than a non-McICA scheme. In the tropics (shown in Figure 12 as $10^oN - 30^oS$ for January), this increase in downward short-wave radiation at the surface (Fig. 12a) is not compensated by an increased loss of long-wave radiation due to a more transparent atmosphere (Fig. 12b). Resulting effect is a heating of the land surface (Fig. 12c), making the atmosphere more unstable above and increasing the convection and subsequent precipitation (Fig. 12d). This also impacts the cloudiness. Over Africa, a reduction in low-level cloudiness is accompanied by an increase in low-level cloudiness eastward (Fig. 12e). Over South America, the reduction in low-level cloudiness over the east of the Amazon Basin does not translate into any clear signal. For total cloudiness (Fig. 12f), the signal is even less apparent as some vertical arrangement occurs with a reduction low-level cloudiness often corresponding to an increase in upper-level cloudiness.

The increase in surface solar radiation over the tropical continents is reflected in the temperature (Fig. 13a), humidity (Fig. 13b) and cloudiness (Fig. 13c).

Over the whole tropical belt, a slight increase in temperature is seen between about 650 and 250 hPa, and a decrease in temperature is seen between 200 hPa. Specific humidity decreases between about 650 and 250 hPa, and increases between 200 and 100 hPa, with a corresponding increase in cloudiness. The impact on the zonal component of the wind (Fig. 14 left) is a weakening of the easterlies in the lower 300 hPa of the atmosphere and of the westerlies between 350 and 100 hPa. Slightly stronger ascent is seen in the vertical velocity (Fig. 14 right) over South America (70^oW), Africa (20^oE) and the Tropical West Pacific (130^oW). Given that in both the long climate simulations at T_L159 and high resolution forecasts the sea surface temperature is specified, the above changes are mainly driven by a change in the contrast between tropical land

masses and ocean.

In terms of radiation at the top of the atmosphere, the changes in radiative heating profiles, and position of the convective activity directly affect the outgoing long-wave radiation (OLR) and absorbed short-wave radiation (ASR), as can be seen in Figure 15, which presents the changes in OLR and ASR during the first 24 and last 24 hours of the ten-day forecasts started every day at 12UTC over January 2007. In the tropical area, the decrease in OLR (a negative quantity) and increase in ASR (a positive quantity) are consistent with more high level cloudiness over South America, South of Africa and the Tropical West Pacific. Impact over Sahara is linked to the revised surface albedo.

The changes brought by McRad (mainly improvements in the climate simulations, and a more realistic distribution of cloudiness in high resolution forecasts from the start of the forecast) can be seen in various objective scores. Figure 16 presents the time series of the difference in r.m.s. error in geopotential at 200, 500 and 1000 hPa for the Northern hemisphere, European area and Southern hemisphere computed over the period 20061201-20070430. A small but systematic improvement is seen over most of the ten days of the forecasts and for all heights and areas. The improvement in the location of the major tropical cloud systems has a direct impact on the tropical scores as seen in Figure 17 for the r.m.s. error of the vector wind at four heights within the troposphere and four lead times (after one, three, five and seven days in the forecasts).

b. Impact on medium resolution 15-day forecasts as used in the EPS

As discussed in Buizza et al. (1999), for each of the 50 forecast members of the EPS, the model uncertainties deriving from parametrized physical processes are simulated by applying a random number between 0.5 and 1.5 to the sum of the physical tendencies within a 10^ox10^o degree

box over three hours. The scaled physical tendencies are then passed to the thermodynamic equation to be solved. Therefore, introducing a more approximate treatment of the radiation tendencies (as through the use of a more reduced radiation grid) is not likely to deteriorate the quality of the EPS forecasts. Table 4 shows the various radiation resolutions from R255 down to R31 that could be used for the current $T_L399L62$ EPS configuration.

In ten-day forecasts with McRad running the $T_L399L62$ model with various resolutions for the radiation grid, the impact on the objective scores was small. For example, Figure 18 presents the r.m.s. error of the temperature at 850 and 200 hPa (the most sensitive parameter) in the Tropics for sets of 93 forecasts starting every fourth day spanning a year from 20060202 to 20070205. For these sets of forecasts with the resolution of the radiation grid being reduced from R255 to R31, the impact on the geopotential is small and does not appear before day 6 of the forecasts (not shown). Similarly small is the impact on the r.m.s. error of temperature at 850 and 200 hPa. Only the mean error in temperature at 850 hPa for all areas (Northern and Southern hemispheres, tropical area) and the mean error in temperature at 200 hPa in the Tropics show a distinct signal. However, the difference between R255 and R31 (i.e, a radiation grid coarsening from $[0.70^o]^2$ to $[5.625^o]^2$) is at most 0.06 K, with the resolutions between R255 and R63 very close to each other, and R47 and R31 showing a more undesirable impact. In the tropics, where these differences in temperature between the various radiation grids are the most marked, the impact on the wind is very small (not shown). So it appears that reducing somewhat the radiation grid could allow for a decreased cost of the EPS with a rather small effect on its overall quality. Further tests were conducted within the VarEPS system running for 10 days at T_L399, then at T_L255 for the last five days using three sets of radiation grids: R159/R95, R95/R63, R47/R31 respectively. Ensemble forecasts were started every 2 days between 3 Dec 2006 and 2 Jan 2007 (16 cases). As shown in Fig. 19, R47/R31 indeed produces an obvious deterioration of the ranked probability skill score of the temperature at 850 hPa in the Southern

hemisphere. The EPS, operational since 5 June 2007, is therefore run at $T_L399L62R95$ then at $T_L255L62R63$.

5. Conclusions and perspectives

The new radiation package McRad presented in this paper became operational with model cycle 32R2 on 5 June 2007. As some previous versions of the ECMWF radiation schemes, McRad will be the radiation scheme used in a future reanalysis. Consequently, this paper is aiming at documenting its main impact on various configurations of the ECMWF IFS.

McRad includes a new short-wave radiation scheme, revised cloud optical properties, the MODIS-derived land surface albedo, the McICA approach to radiation transfer in cloudy atmospheres, and a more extensive use of a flexible radiation grid that can be made coarser for all applications, but particularly useful when the highest accuracy of the radiative heating rates, as with the EPS, is not essential for the application.

The impact of McRad was studied in seasonal simulations and ten-day forecasts, and it was shown to benefit the representation of most parameters at both short and longer time-scales, relative to the previous operational version of the RT schemes. McRad was shown to improve the signatures of the clouds on the top of the atmosphere radiation budget, both in terms of their amplitude but also in terms of their location. McRad modifies the relative vertical distributions of the long-wave and short-wave radiative heating and the amount of short-wave radiation reaching the surface. These changes directly impact the structure of the planetary boundary-layer (seen in the change in low-level cloudiness) and the strength of the convection (seen in the change in outgoing long-wave radiation and precipitation). By allowing more convection over the tropical continents, McRad indirectly modifies the large-scale Hadley and Ferrel circulation

as seen in the changes in low-level wind over the tropical oceans. All these changes mostly improve the behaviour of the model at both short and longer time-scales. At short time-scales, the McRad forecasts are in better agreement than the operational forecasts with respect to their own analyses, as seen in the reduced r.m.s. errors in geopotential and wind.

With respect to surface albedo, the MODIS-derived land surface albedo is at present not used for the ice-covered Greenland and Antarctica. By the same token, the definition of the sea-ice albedo has not been revised. Revision of the albedo over these areas will be considered in the future.

Up to this point in the paper, $RRTM_{SW}$ has been advocated as a scheme very suitable for the McICA approach due to the large number of spectral computations. However, $RRTM_{SW}$ has merits on its own. With the McRad package, both the LW and SW radiation schemes are based on the same line-by-line model and the same database of spectroscopic parameters. As part of ARM (Atmospheric Radiation Measurement program of the US DoE), both the $RRTM_{LW}$ and $RRTM_{SW}$ models (and the corresponding line-by-line model LBLRTM, Clough et al., 1992; Clough and Iacono, 1995) have been extensively used these last three or four years for sustained comparisons against spectrometer measurements at the ARM South Great Plains (SGP), North Slope of Alaska (NSA) and two Tropical West Pacific sites. When profiles of the quantities governing the radiation transfer are taken from measurements, the agreement between one-hour averaged computed and observed radiation fluxes at both top and bottom of the atmosphere is better than 2 Wm^{-2} in LW and 10 Wm^{-2} in SW in clear-sky/aerosol only conditions and 5 Wm^{-2} and 25 Wm^{-2} in cloudy conditions, at least a factor of 5 better than the best RT schemes at the end of '90s.

In terms of methodology, McICA is the most important change as it simplifies the radiation transfer schemes by suppressing all references to partial cloud cover, avoids separate calcula-

tions for clear-sky and cloudy parts of the layers, and gets rid of the inherent complexity of the vertical integration accounting for the overlapping of these clear and cloudy quantitites (reflectances/transmittances or fluxes). The cloud generator used here (Räisänen et al., 2004) being independent of the radiation transfer can now handle any overlap situation, and is used here with a definition of the overlap of cloud layers through decorrelation lengths (Hogan and Illingworth, 2000, 2003). It must again be stressed that, through McICA, McRad is ready to handle implicitly any spatial inhomogeneity (horizontal and/or vertical) in the distribution of the condensed water in clouds. The McICA approach could also be used for dealing with inhomogeneities in surface boundary conditions, a feature that could be of importance when the radiation fluxes are computed over an area encompassing several model grids, each with a number of tiles with different long-wave emissivity and short-wave albedo.

McRad will allow the same overlap assumption to be used for radiation transfer and precipitation/evaporation processes, a problem previously solved either only approximately (Jakob and Klein, 1999, 2000) or through additional calculations. In the future, it will help connect the radiation transfer calculations with cloud information derived from pdf-based cloud schemes (as that of Tompkins, 2002) (thanks to the McICA approach) and from observations of the vertical profiles of the condensed water as made available from CALIPSO-type measurements (thanks to the flexible handling of cloud overlap). As it does for cloud information, McRad can also include information on the sub-grid variablility of the water vapour that would be provided by a pdf-based cloud scheme working on total water.

Acknowledgments

A number of other people helped in various aspects of this study. P. Räisäinen (FMI) wrote the cloud generator. E. Mlawer, J. Delamere, and A. Clough (AER, Inc.) originally contributed

to the development of both the original RRTM long-wave and short-wave radiation codes that were later modified to run at ECMWF and to include the McICA approximation to deal with cloudiness. MODIS data processed in terms of components of the surface albedo were obtained from C. Schaaf at Boston University. At ECMWF, G. Mozdzynski originally developed the reduced grid concept, and applied it to radiation computations. D. Salmond and J. Hague helped in the debugging and optimization of various codes. S. Serrar helped implement the MODIS albedo. M. Leutbecher ran the EPS experiments and discussed the results. A. Weisheimer and F. Doblas-Reyes ran the integrations with the coupled ocean model. P. Bougeault, M. Miller, and A. Beljaars are thanked for their comments on this paper. RP's work was supported by the Office of Science (BER), U.S. Department of Energy (Grant DE-FG02-03ER63561).

REFERENCES

Barker, H.W., G.L. Stephens, and Q. Fu, 1999: The sensitivity of domain-averaged solar fluxes to assumptions about cloud geometry. *Quart. J. Roy. Meteor. Soc.*, **125**, 2127-2152.

Barker, H.W., R. Pincus, and J.-J. Morcrette, 2002: The Monte-Carlo Independent Column Approximation: Application within large-scale models. *Proceedings GCSS/ARM Workshop on the Representation of Cloud Systems in Large-Scale Models*, May 2002, Kananaskis, Al, Canada, 10 pp. http://www.met.utah.edu/skrueger/gcss-2002/Extended-Abstracts.pdf

Barker, H.W., G.L. Stephens, P.T. Partain, and J.-J. Morcrette among 29 others, 2003: Assessing 1D atmospheric solar radiative transfer models: Interpretation and handling of unresolved clouds. *J. Climate*, **16**, 2676-2699.

Buizza, R., M.J. Miller and T.N. Palmer, 1999: Stochastic representation of model uncertainties in the ECMWF Ensemble Prediction System. *Quart. J. Roy. Meteor. Soc.*, **125**, 2887–2908.

Cahalan, R.F., W. Ridgway, W.J. Wiscombe, and T.L. Bell, 1994: The albedo of fractal stratocumulus clouds. *J. Atmos. Sci.*, **51**, 2434-2455.

Cairns, B., A.A. Lacis, and B.E. Carlson, 2000: Absorption within inhomogeneous clouds and its parameterization in general circulation models. *J. Atmos. Sci.*, **57**, 700-714.

Clough, S.A., M.I. Iacono, and J.-L. Moncet, 1992: Line-by-line calculations of atmospheric fluxes and cooling rates: Application to water vapor. *J. Geophys. Res.*, **97D**, 15761-15786.

Clough, S.A., and M.I. Iacono, 1995: Line-by-line calculation of atmospheric fluxes and cooling rates, 2, Application to carbon dioxide, ozone, methane, nitrous oxide and the halocarbons. *J. Geophys. Res.*, **100D**, 16519-16536.

Clough, S.A., M.W. Shephard, E.J. Mlawer, J.S. Delamere, M.J. Iacono, K. Cady-Pereira, S. Boukabara, P.D. Brown, 2005: Atmospheric radiative transfer modeling: a summary of the AER codes, *J. Quant. Spectrosc. Radiat. Transfer*, **91**, 233-244.

Da Silva, A.M., and S. Levitus, 1994: *Atlas of surface marine data. Vol. I: Algorithms and procedures.* National Oceanic and Atmospheric Administration. NOAA Atlas NESDIS **6**, Washington DC, USA, 83 pp.

Ebert, E.E., and J.A. Curry, 1992: A parametrisation of ice cloud optical properties for climate models. *J. Geophys. Res.*, **97D**, 3831-3836.

Fouquart, Y., 1987: *Radiative transfer in climate models*. NATO Advanced Study Institute on Physically-Based Modelling and Simulation of Climate and Climatic Changes. Erice, Sicily, 11-23 May 1986. M.E. Schlesinger, Ed., Kluwer Academic Publishers, 223-284.

Fouquart, Y., and B. Bonnel, 1980: Computations of solar heating of the earth's atmosphere: a new parameterization. *Beitr. Phys. Atmosph.*, **53**, 35-62.

Fouquart, Y., B. Bonnel, and V. Ramaswamy, 1991: Intercomparing shortwave radiation codes for climate studies. *J. Geophys. Res.*, **96D**, 8955-8968.

Fu, Q., 1996: An accurate parameterization of the solar radiative properties of cirrus clouds for climate studies. *J. Climate*, **9**, 2058-2082.

Fu, Q., P. Yang, and W.B. Sun, 1998: An accurate parameterization of the infrared radiative properties of cirrus clouds of climate models. *J. Climate*, **11**, 2223-2237.

Geleyn, J.-F., 1977: A comprehensive radiation scheme designed for fast computation. ECMWF Research Dept. Internal Report No. 8, 36 pp.

Geleyn, J.-F., and A. Hollingsworth, 1979: An economical analytical method for the computation of the interaction between scattering and line absorption of radiation. *Beitr. Phys. Atmosph.*, **52**, 1-16.

Hogan, R.J., and A.J. Illingworth, 2000: Deriving cloud overlap statistics from radar. *Quart. J. Roy. Meteor. Soc.*, **126**, 2903-2909.

Hogan, R.J. and A.J. Illingworth, 2003: Parameterizing ice cloud inhomogeneity and the overlap of inhomogeneities using cloud radar data. *J. Atmos. Sci.*, **60**, 756-767 .

ICRCCM, The InterComparison of Radiation Codes in Climate Models, 1991: *J. Geophys. Res.*, **96D**, 8921-9158 (16 papers).

Jakob, C., and S.A. Klein, 1999: The role of vertically varying cloud fraction in the parametrization of microphysical processes in the ECMWF model. *Quart. J. Roy. Meteor. Soc.*, **125**, 941-965.

Jakob, C., and S.A. Klein, 2000: A parametrization of the effects of cloud and precipitation overlap for use in general circulation models. *Quart. J. Roy. Meteor. Soc.*, **126**, 2525-2544.

Lacis, A.A., and V. Oinas, 1991: A description of the correlated-k distribution method for modeling nongray gaseous absorption, thermal emission, and multiple scattering in vertically inhomogeneous atmospheres. *J. Geophys. Res.*, **96D**, 9027-9063.

Li, J., 2002: Accounting for unresolved clouds in a 1D infrared radiative transfer code. Part I: Solution for radiative transfer , including cloud scattering and overlap. *J. Atmos. Sci.*, **59**, 3302-3320.

Lindner, T.H., and J. Li, 2000: Parameterization of the optical properties for water clouds in the infrared. *J. Climate*, **13**, 1797-1805.

Martin, G.M., D.W. Johnson, and A. Spice, 1994: The measurement and parameterization of effective radius of droplets in warm stratocumulus. *J. Atmos. Sci.*, **51**, 1823-1842.

Mlawer, E.J., and S.A. Clough, 1997: Shortwave and longwave enhancements in the Rapid Radiative Transfer Model, in Proceedings of the 7th Atmospheric Radiation Measurement (ARM) Science Team Meeting, U.S. Department of Energy, CONF-9603149.
http://www.arm.gov/publications/proceedings/conf07/title.stm/mlaw-97.pdf

Mlawer, E.J., S.J. Taubman, P.D. Brown, M.J. Iacono, and S.A. Clough, 1997: Radiative transfer for inhomogeneous atmospheres: RRTM, a validated correlated-k model for the longwave. *J. Geophys. Res.*, **102D**, 16,663-16,682.

Morcrette, J.-J., and Y. Fouquart, 1986: The overlapping of cloud layers in shortwave radiation parameterizations. J. Atmos. Sci., 43, 321-328.

Morcrette, J.-J., 1990: Impact of changes to the radiation transfer parameterizations plus cloud optical properties in the ECMWF model. *Mon. Wea. Rev.*, **118**, 847-873.

Morcrette, J.-J., 1991: Radiation and cloud radiative properties in the ECMWF operational

weather forecast model. *J. Geophys. Res.*, **96D**, 9121-9132.

Morcrette, J.-J., 1993: Revision of the clear-sky and cloud radiative properties in the ECMWF model. *ECMWF Newsletter*, **61**, 3-14.

Morcrette, J.-J., S.A. Clough, E.J. Mlawer, and M.J. Iacono, 1998: Impact of a validated radiative transfer scheme, RRTM, on the ECMWF model climate and 10-day forecasts. ECMWF Technical Memo. No. 252, 47 pp.

Morcrette, J.-J., 2000: On the effects of the temporal and spatial sampling of radiation fields on the ECMWF forecasts and analyses. *Mon. Wea. Rev.*, **128**, 876-887.

Morcrette, J.-J., and C. Jakob, 2000: The response of the ECMWF model to changes in cloud overlap assumption. *Mon. Wea. Rev.*, **128**, 1707-1732.

Morcrette, J.-J., E.J. Mlawer, M.J. Iacono, and S.A. Clough, 2001: Impact of the radiation transfer scheme RRTM in the ECMWF forecasting system. *ECMWF Newsletter*, **91**, 2-9.

Morcrette, J.-J., 2002a: Assessment of the ECMWF model cloudiness and surface radiation fields at the ARM-SGP site. *Mon. Wea. Rev.*, **130**, 257-277.

Morcrette, J.-J., 2002b: The surface downward longwave radiation in the ECMWF forecast system. *J. Climate*, **15**, 1875-1892.

Oreopoulos, L. and H. W. Barker, 1999: Accounting for subgrid-scale cloud variability in a multi-layer 1D solar radiative transfer algorithm. *Quart. J. Roy. Meteor. Soc.*, **125**, 301-330.

Ou, S.C., and K.-N. Liou, 1995: Ice microphysics and climatic temperature feedback. *Atmosph. Research*, **35**, 127-138.

Pincus, R., H.W. Barker, and J.-J. Morcrette, 2003: A fast, flexible, approximate technique for computing radiative transfer in inhomogeneous clouds. *J. Geophys. Res.*, 108D, 4376,

doi:10.1029/2002JD003322.

Räisänen, P., and. H.W. Barker, 2004: Evaluation and optimization of sampling errors for the Monte Carlo Independent Column Approximation. *Quart. J. Roy. Meteor. Soc.*, **130**, 2069-2085.

Räisänen, P., H.W. Barker, M. Khairoutdinov, J. Li, and D.A. Randall, 2004: Stochastic generation of subgrid-scale cloudy columns for large-scale models. *Quart. J. Roy. Meteor. Soc.*, **130**, 2047-2067.

Räisänen, P., G.A. Isaac, H.W. Barker, and I. Gultepe, 2003: Solar radiative transfer for stratiform clouds with horizontal variations in liquid water path and droplet effective radius. *Quart. J. Roy. Meteor. Soc.*, **129**, 2135-2149.

Schaaf, C.B., F. Gao, A.H. Strahler, W. Lucht, X. Li, T. Tsang, N.C. Strugnell, X. Zhang, Y. Jin, J.-P. Muller, P. Lewis, M. Barnsley, P. Hobson, M. Disney, G. Roberts, M. Dunderdale, C. Doll, R.P. d'Entremont, B. Hu, S. Liang, J.L. Privette, and D. Roy, 2002: First operational BRDF, albedo nadir reflectance products from MODIS. *Remote Sensing Environm.*, **83**, 135-148.

Sellers, P.J., S.O. Los, C.J. Tucker, C.O. Justice , D.A. Dazlich, G.J. Collatz and D.A. Randall, 1996: Part II: The generation of global fields of terrestrial biophysical parameters from satellite data. *J. Climate*, **9**, 706-737.

Senior, C.A., 1999: Comparison of mechanisms of cloud-climate feedbacks in GCMs. *J. Climate*, **12**, 1480-1489.

Slingo, A., 1989: A GCM parameterization for the shortwave radiative properties of water clouds. *J. Atmos. Sci.*, **46**, 1419-1427.

Slingo, J.M., 1987: The development and verification of a cloud prediction scheme for the

ECMWF model. *Quart. J. Roy. Meteor. Soc.*, **113**, 899-928.

Smith, E.A., and L. Shi, 1992: Surface forcing of the infrared cooling profile over the Tibetan plateau. Part I: Influence of relative longwave radiative heating at high altitude. *J. Atmos. Sci.*, **49**, 805-822.

Stephens, G.L., 1988: Radiative transfer through arbitrarily shaped optical media: Part I: A general method of solution. *J. Atmos. Sci.*, **45**, 1818-1836.

Sun, Z., 2001: Reply to comments by G.M. McFarquhar on "Parametrization of effective sizes of cirrus-cloud particles and its verification against observations". *Quart. J. Roy. Meteor. Soc.*, **127A**, 267-271.

Tiedtke, M., 1993: Representation of clouds in large-scale models. *Mon. Wea. Rev.*, **121**, 3040-3061.

Tiedtke, M., 1996: An extension of cloud-radiation parameterization in the ECMWF model: The representation of sub-grid scale variations of optical depth. *Mon. Wea. Rev.*, **124**, 745-750.

Tompkins, A.M., 2002: A prognostic parameterization for the sub-grid scale variability of water vapor and clouds in large-scale models and its use to diagnose cloud cover. *J. Atmos. Sci.*, **59**, 1917-1942.

Uppala, S.M., et al. 2005: The ERA-40 re-analysis. *Quart. J. R. Meteor. Soc.*, **131**, 2961-3012.

TABLE CAPTIONS:

Table 1: Major changes in the representation of radiation transfer in the ECMWF forecasting system.

Table 2: Annual means from 13-month cycle OPE simulations (first month is discarded) at $T_L159L91$ with the ERBE- and MODIS-derived land surface albedos. Radiative fluxes at the top of the atmosphere (TOA) are compared to CERES measurements: OLR is the outgoing long-wave radiation, ASW is the net short-wave radiation, LWCF and SWCF the long-wave and short-wave cloud forcing, respectively, all in $W\ m^{-2}$. TP is the total precipitation (mm/day) compared to GPCP data. For the model, bias and standard deviation (between parentheses) are given for the previously operational Rad and McRad models.

Table 3: Characteristics of the long-wave and short-wave radiation schemes in McRad.
(+) refer to the configuration operational up to CY31R2
(*) refer to the configuration operational with McRad.

Table 4: Impact of the McRad radiation package on the timing of the ECMWF model forecasts for different configurations and different horizontal resolutions. Dyn is the resolution for the dynamics, Rad that for the radiation. $Freq$ is the frequency (hour) for calling the full radiation scheme, $\%Rad$ is the fraction of computer time taken by the radiative transfer calculations. $Ratio$ is the factor by which McRad increases the computer cost relative to the previous operational configuration (OPE). (*) refers to the operational configuration implemented on 5 June 2007.

Table 5: Annual means from 13-month simulations at $T_L159L91$, discarding the first month. Radiative fluxes at TOA are compared to CERES measurements, total cloud cover (TCC in percent) to ISCCP D2 data, total column water vapour (TCWV in $kg\ m^{-2}$) and liquid water

(TCLW in $g\ m^{-2}$) to SSM/I data. TP is the total precipitation (in $mm\ day^{-1}$) compared to GPCP or over ocean to SSM/I data. The surface fluxes over the ocean (in $W\ m^{-2}$) are compared to the Da Silva-Levitus climatology, with SSR and STR the surface net solar and terrestrial radiation, respectively, SSH and SLH, the surface sensible and latent heat fluxes, respectively, and SNET the surface net energy flux. For the model, bias and standard deviation (between parentheses) are given for the previously operational and McRad models. At the top of the atmosphere, OLR is the outgoing long-wave radiation, ASW is the net short-wave radiation, LWCF and SWCF the long-wave and short-wave cloud forcing, respectively, all in $W\ m^{-2}$.

Table 6: Results from 13-month cycle OPE simulations at $T_L159L91$ with different cloud configurations. $G21$ is the McRad model with generalized overlap of cloud layers with a decorrelation length for cloud cover DLCC=2 km and and a decorrelation length for cloud water DLCW=1 km, G42 is with DLCC=4 km and DLCW=2 km, G51 with DLCC=5 km and DLCW=1 km. MR is the McRad model with maximum-random overlap of homogeneous clouds. All quantities are annual means. Radiative fluxes at TOA are compared to CERES measurements, total cloud cover (TCC) to ISCCP D2 data, total column water vapour (TCWV) and liquid water (TCLW) to SSM/I data. TP is the total precipitation compared to GPCP or SSM/I data (over ocean). The surface fluxes are compared to the Da Silva-Levitus climatology.

Cycle	Date of implementation	Description
SPM 32	02/05/1989	RT schemes from Univ.Lille
SPM 46	01/02/1993	Optical properties for ice and mixed phase clouds
IFS 14R3	13/02/1996	Revised LW and SW absorption coefficients from HITRAN'92
IFS 16R2	15/05/1997	Voigt profile in long-wave RT scheme
IFS 16R4	27/08/1997	Revised ocean albedo from ERBE
IFS 18R3	16/12/1997	Revised LW and SW absorption coefficients from HITRAN'96
IFS 18R5	01/04/1998	Seasonal land albedo from ERBE
IFS 22R3	27/06/2000	$RRTM_{LW}$ as long-wave RT scheme
		short-wave RT scheme with 4 spectral intervals
IFS 23R4	12/06/2001	Hourly, instead of 3-hourly, calls to RT code during data assimilation cycle
IFS 25R1	09/04/2002	Short-wave RT scheme with 6 spectral intervals
IFS 26R3	07/10/2003	New aerosol climatology adapted from Tegen et al. (1997)
IFS 28R3	28/09/2004	Radiation called hourly in high resolution forecasts
IFS 32R2	05/06/2007	McICA approach to RT with $RRTM_{LW}$ and $RRTM_{SW}$
		revised cloud optical properties, MODIS-derived land albedo

Table 1:

	OLR	ASW	LWCF	SWCF	TP
Observ.	-239	244	27.3	-48.7	2.61
Rad ERBE	-8.1 (12.7)	-10.0 (17.5)	-9.6 (13.6)	-5.2 (15.4)	0.45 (1.39)
Rad MODIS	-8.4 (12.8)	-10.2 (17.0)	-9.8 (13.8)	-5.3 (15.1)	0.42 (1.30)
McRad ERBE	-3.4 (8.3)	-6.3 (14.7)	-4.2 (8.2)	-0.0 (13.1)	0.42 (1.30)
McRad MODIS	-3.2 (7.9)	-5.8 (14.2)	-4.0 (7.9)	-0.2 (12.9)	0.40 (1.21)

Table 2:

	$RRTM_{LW}$	$RRTM_{SW}$
Solution of RT Equation	two-stream method	two-stream method
Number of spectral intervals	16 (140 g-points)	14 (112 g-points)
Absorbers	H_2O, CO_2, O_3, CH_4, N_2O, $CFC11$, $CFC12$, aerosols	H_2O, CO_2, O_3, CH_4, N_2O, $CFC11$, $CFC12$, aerosols
Spectroscopic database	HITRAN, 1996	HITRAN, 1996
Absorption coefficients	from LBLRTM line-by-line model	from LBLRTM line-by-line model
Cloud handling	true cloud fraction	true cloud fraction
Cloud overlap assumption as set up in cloud generator	maximum-random (+) generalized (*)	maximum-random (+) generalized (*)
Cloud optical properties		
method	16-band spectral emissivity from τ, g, ω	14-band τ, g, ω
Data: ice clouds water clouds	Ebert & Curry, 1992 (+) Fu et al., 1998 (*) Smith & Shi, 1992 (+) Lindner & Li, 2000 (*)	Ebert & Curry, 1992 (+) Fu, 1996 (*) Fouquart, 1987 (+) Slingo, 1989 (*)
Effective liquid droplet size Effective ice particle size	Martin et al., 1994 Sun, 2001	Martin et al., 1994 Sun, 2001
Reference	Mlawer et al., 1997 Morcrette et al., 2001	Clough et al., 2005

Table 3:

Configuration	Dyn	Rad	Freq	%Rad	Ratio
$T_L799L91$					
OPE	799	399	1	7.3	1.000
McRad	799	511	1	36.4	1.456
	799	399	1	26.5	1.262
	799	319(*)	1	19.2	1.147
	799	255	1	13.8	1.076
	799	159	1	6.7	0.994
	799	95	1	3.4	0.960
$T_L399L62$					
OPE	399	159	3	4.1	1.000
McRad	399	255	3	31.6	1.403
	399	159	3	16.4	1.148
	399	95(*)	3	7.7	1.039
	399	63	3	3.8	0.998
	399	47	3	3.0	0.989
	399	31	3	2.1	0.980
$T_L159L91$					
OPE	159	63	3	8.0	1.000
McRad	159	159	3	67.5	2.831
	159	95	3	45.1	1.675
	159	63(*)	3	27.7	1.273
	159	47	3	19.5	1.143
	159	31	3	11.0	1.034

Table 4:

	Annual	DJF	JJA
OLR	-239	-236	-242
OPE	-8.1 (12.7)	-6.1 (15.0)	-5.1 (12.8)
McRad	-3.2 (7.9)	-1.1 (10.1)	-0.6 (10.5)
ASW	244	251	238
OPE	-10.0 (17.5)	-15.6 (23.9)	-9.2 (19.7)
McRad	-5.8 (14.2)	-11.4 (20.5)	-5.3 (18.6)
LWCF	27.3	26.8	26.1
OPE	-9.6 (13.6)	-10.4 (16.5)	-8.3 (14.1)
McRad	-4.0 (7.9)	-4.8 (10.3)	-3.0 (9.7)
SWCF	-48.7	-52.8	-45.1
OPE	-5.2 (15.4)	-4.1 (18.6)	-6.3 (18.2)
McRad	-0.2 (12.9)	0.5 (17.0)	-1.3 (17.3)
TCC	62.2	62.9	61.4
OPE	-6.0 (10.3)	-5.7 (12.3)	-5.4 (11.8)
McRad	-5.3 (9.5)	-4.9 (11.2)	-4.7 (11.4)
TP gpcp	2.61	2.58	2.63
OPE	0.45 (1.39)	0.42 (1.88)	0.43 (1.75)
McRad	0.40 (1.21)	0.37 (1.60)	0.41 (1.72)
TP ssmi	3.80	3.57	3.66
OPE	0.67 (2.45)	0.57 (3.56)	0.44 (3.90)
McRad	0.50 (2.23)	0.38 (3.32)	0.35 (3.81)

Table 5:

TCWV	29.0	27.7	29.3
OPE	-2.10 (3.65)	-2.27 (4.29)	-1.73 (3.69)
McRad	-1.67 (3.13)	-1.80 (3.63)	-1.25 (3.32)
TCLW	82.2	80.4	84.3
OPE	1.67 (22.1)	3.13 (33.4)	-1.11 (30.6)
McRad	0.86 (22.4)	2.05 (32.8)	-1.21 (30.8)
SSR ocn	155.2	163.7	143.7
OPE	8.4	15.1	0.3
McRad	15.6	21.9	7.4
STR ocn	-51.8	-52.5	-50.4
OPE	0.6	1.0	1.3
McRad	-0.1	0.3	0.6
SSH ocn	-11.0	-13.7	-9.0
OPE	-4.7	-3.0	-5.9
McRad	-3.5	-2.0	-4.9
SLH ocn	-96.5	-100.2	-94.2
OPE	-10.5	-7.7	-11.1
McRad	-7.2	-4.5	-7.9
SNET ocn	-2.1	-0.9	-7.9
OPE	-8.1	3.6	-17.3
McRad	2.8	14.0	-6.8

Table 5: continued

	Observation	G21	G42	G51	MR
OLR	-239	-2.7 (7.8)	-4.3 (8.1)	-3.9 (7.8)	0.02 (8.3)
ASW	244	-5.9 (14.6)	-1.8 (12.5)	-1.9 (12.3)	-13.1 (19.5)
LWCF	27.3	-2.6 (6.9)	-4.0 (7.3)	-3.6 (7.0)	0.03 (7.5)
SWCF	-48.7	-0.2 (13.4)	3.8 (12.6)	-3.7 (12.4)	-7.5 (17.2)
TCWV	29.0	-1.38 (3.06)	-1.43 (3.03)	-1.40 (3.02)	-1.18 (2.92)
TCC	62.2	-1.04 (11.1)	-1.14 (11.0)	-1.00 (10.7)	-0.12 (10.9)
TCLW	82.2	-7.44 (22.7)	-7.45 (22.8)	-7.31 (22.7)	-5.37 (22.2)
TP gpcp	2.61	0.30 (1.17)	0.31 (1.15)	0.30 (1.14)	0.29 (1.19)
TP ssmi	3.80	0.31 (2.16)	0.30 (2.14)	0.26 (2.10)	0.31 (2.23)
SSR ocn	155.2	15.9	20.1	19.9	7.3
STR ocn	-51.8	-3.6	-5.0	-4.9	-0.5
SSH ocn	-11.0	-1.6	-1.6	-1.5	-1.5
SLH ocn	-96.5	-4.2	-4.1	-3.5	-4.1
SNET ocn	-2.1	4.5	7.4	7.9	-0.8

Table 6:

List of Figures

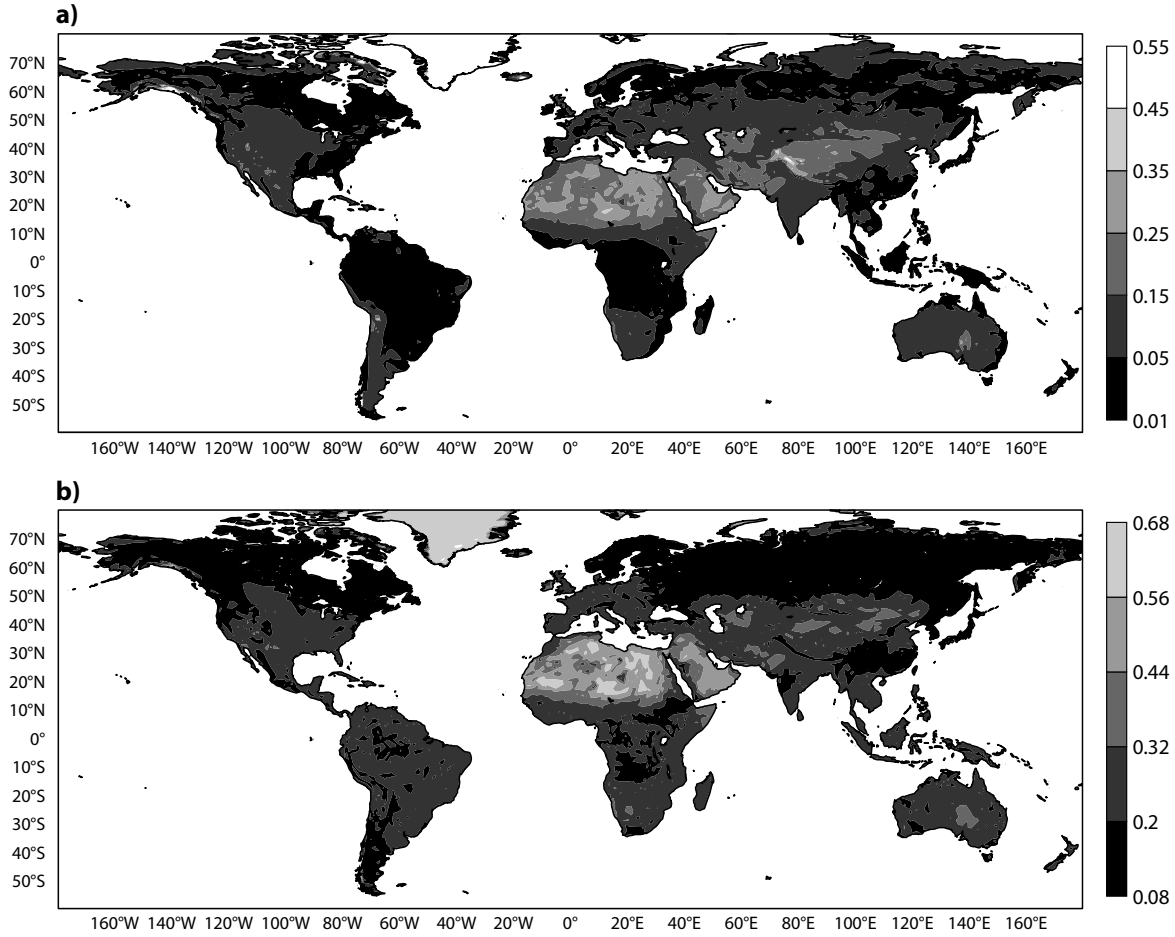

FIG. 1. The land surface albedo derived from MODIS observations for April at T_L799. Top panel is for the UV-visible (0.3-0.7 μm), bottom panel for the near-infrared (0.7-5.0 μm) part of the short-wave spectrum.

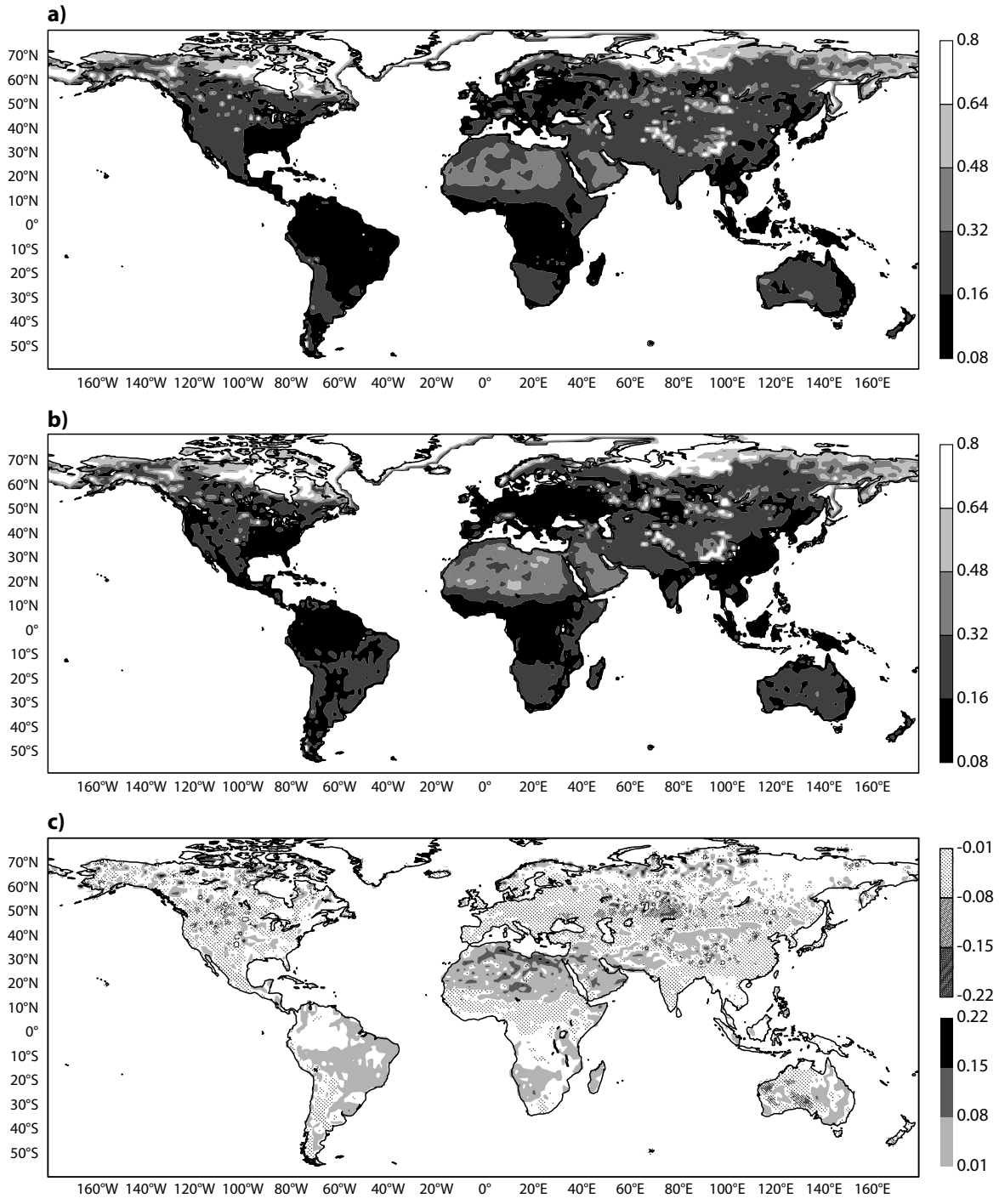

FIG. 2. The land surface albedo over the entire short-wave spectrum for April as seen by the model at T_L799. Top panel is the spectrally flat ERBE-derived albedo, middle panel is the equivalent albedo obtained using the various MODIS-derived albedo components, bottom panel is the difference between the model with MODIS and ERBE albedos.

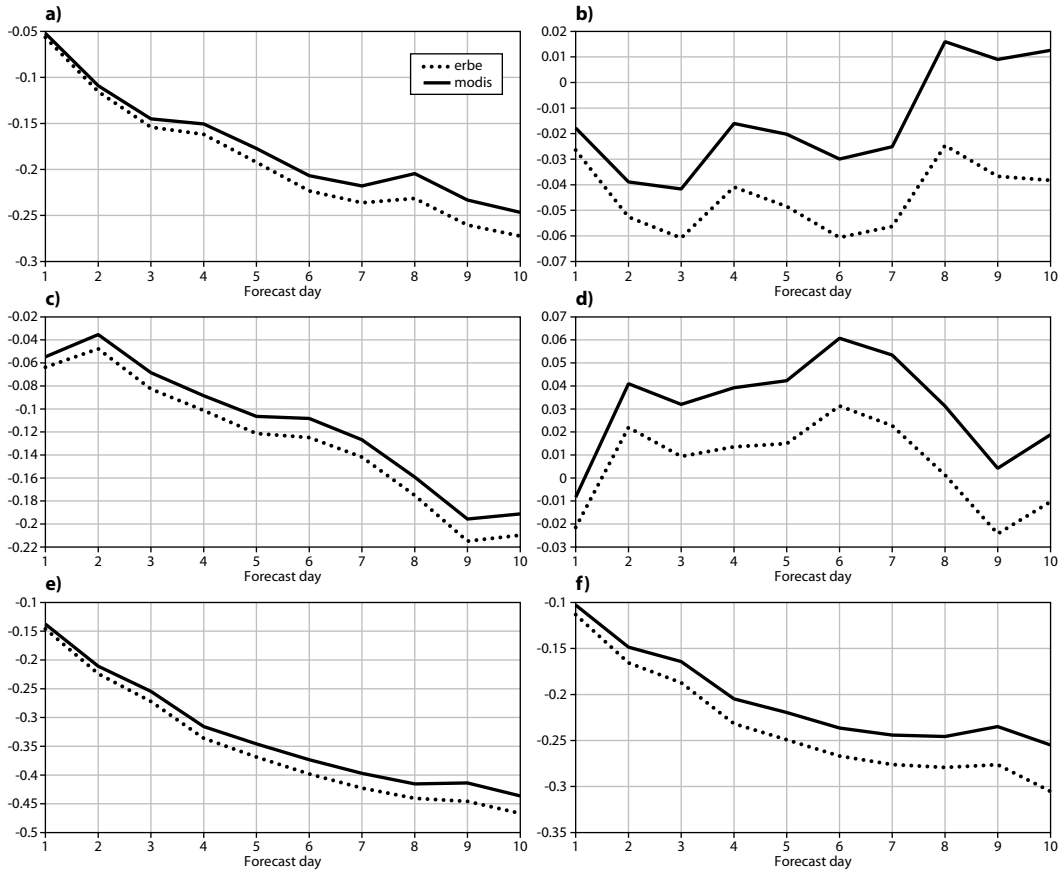

FIG. 3. The mean error of the temperature at 850 hPa for the Northern hemisphere, Tropics, and Southern hemisphere (from top to bottom) from sets of 93 10-day forecasts at $T_L399L62$, started every 96 hours from 2006020212 to 2007020512 with the cycle 32R2 of the ECMWF model. Left panels are for the pre-32R2 radiation configuration, right panels for the 32R2 McRad configuration; red and blue curves correspond to the MODIS-derived and ERBE-derived land surface albedo, respectively.

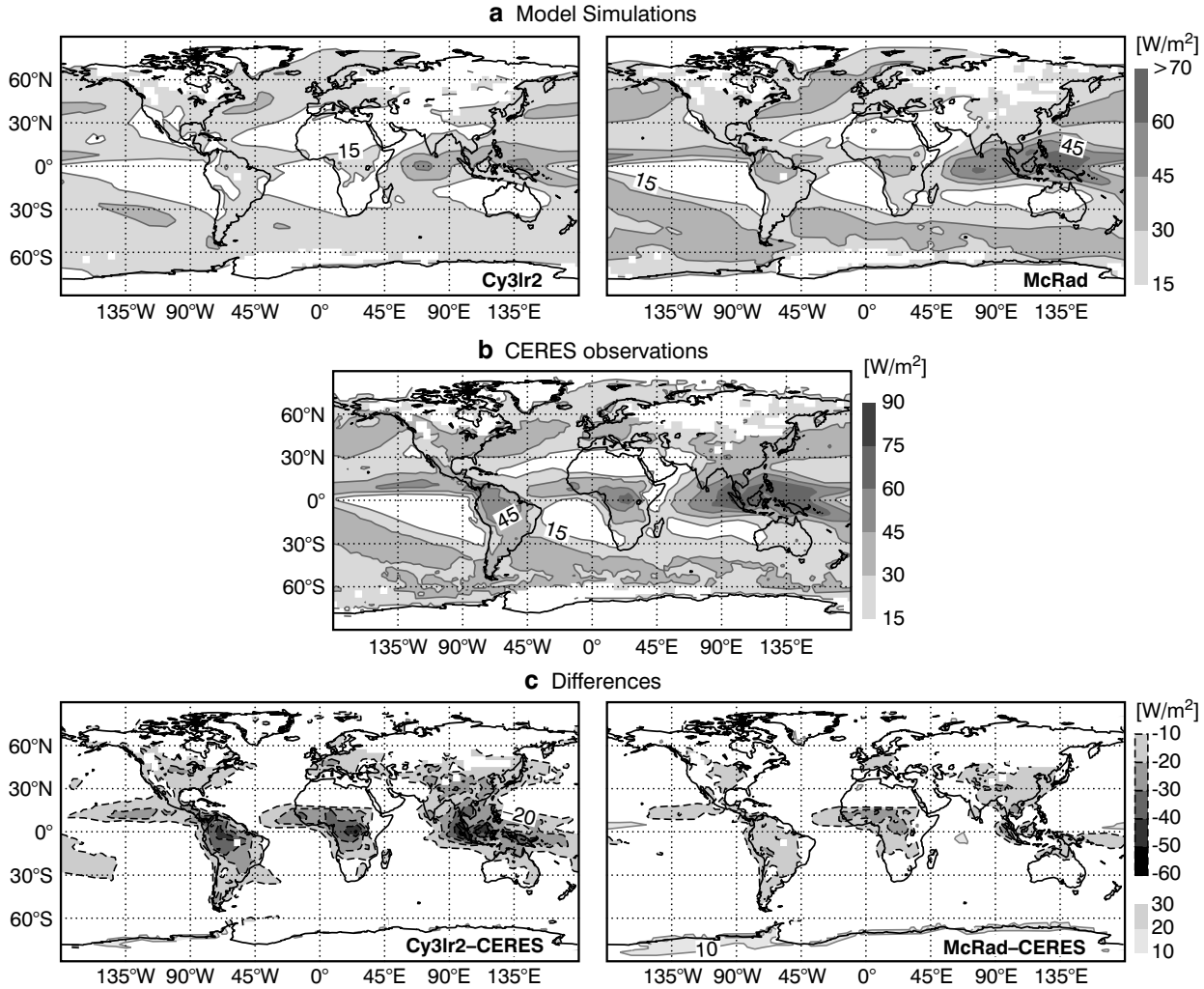

FIG. 4. Annual average of the long-wave cloud forcing (in Wm^{-2}). Top figures are the ECMWF model simulations (left: OPE, right: McRad), middle one is the CERES observations, bottom ones are the differences between simulations and observations. For the model, results are for averages over 3 simulations starting 24 hours apart, with output parameters averaged over the September 2000-August 20001 period.

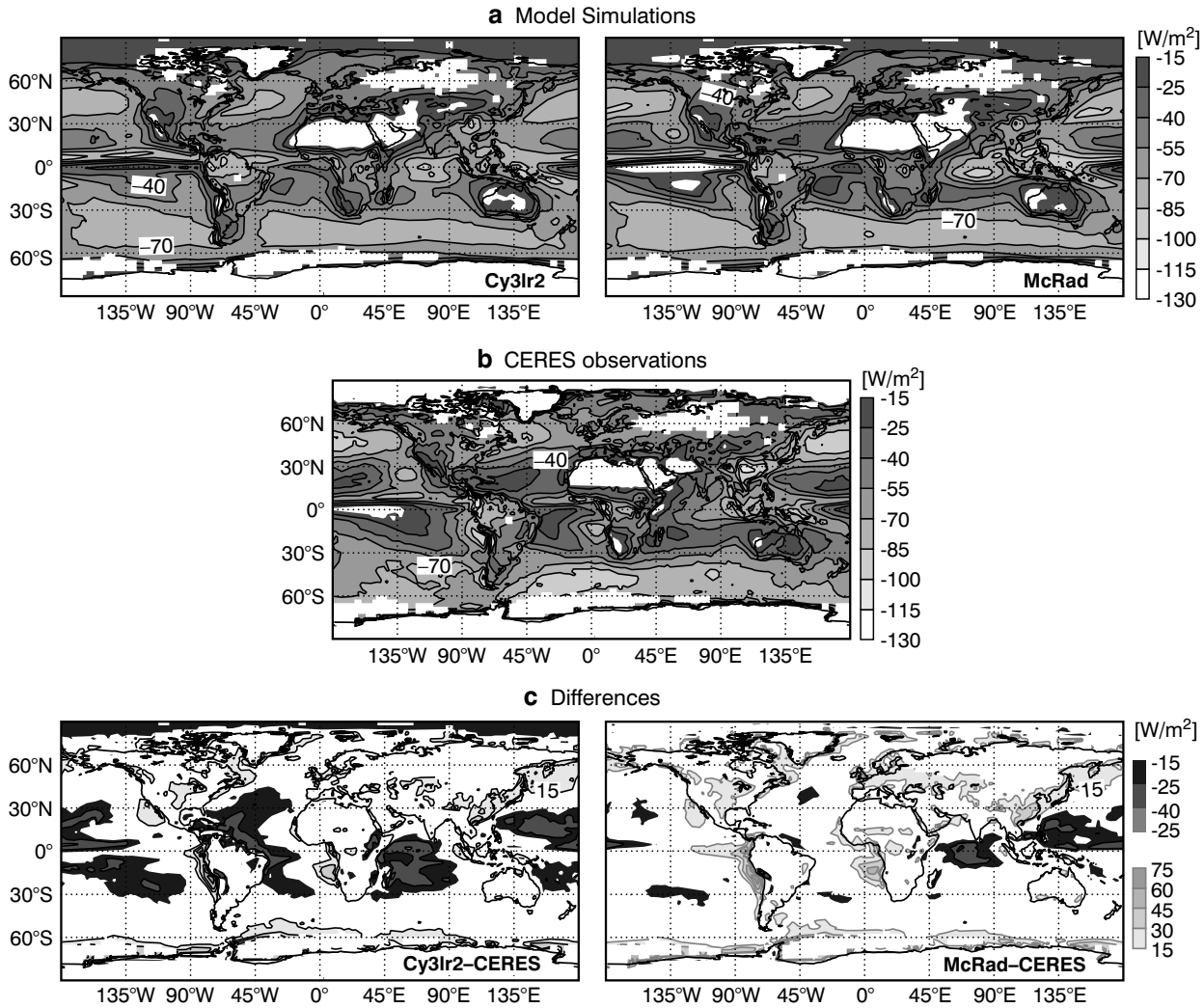

FIG. 5. As in Fig. 4, but for the short-wave cloud forcing (in Wm^{-2}). Top figures are the ECMWF model simulations (left: OPE, right: McRad), middle one is the CERES observations, bottom ones are the differences between simulations and observations.

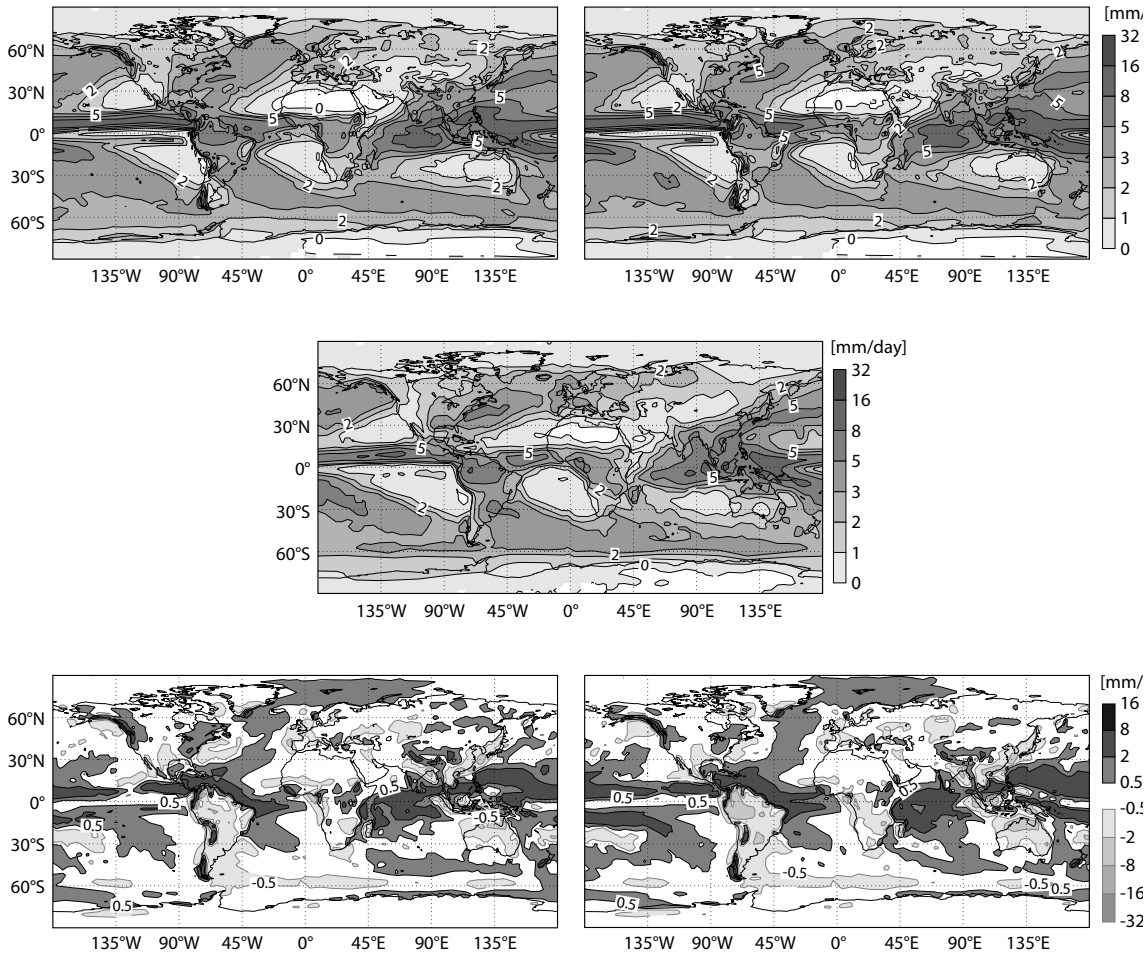

FIG. 6. As in Fig. 4, but for the total precipitation (in $mm\ day^{-1}$). Top figures are the ECMWF model simulations (left: operational, right: McRad), middle one is the GPCP observations, bottom ones are the differences between simulations and observations.

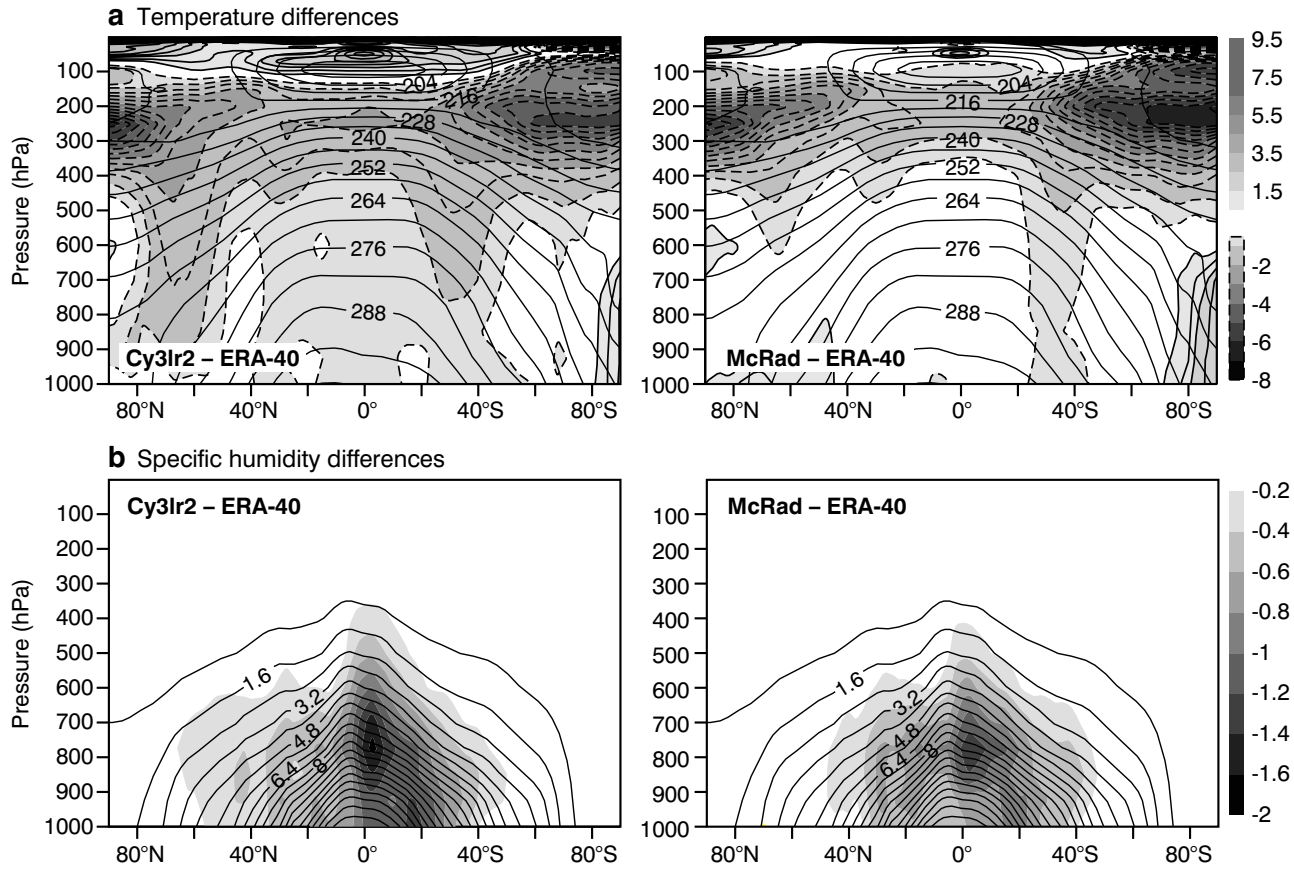

FIG. 7. Zonal mean cross-section of the difference between the McRad model and the ERA40 analysis over the 12-month period September 2000-August 2001. Temperature in the top panels (K) and humidity in the bottom panels ($g\ kg^{-1}$). Left column is for OPE; right one for the McRad model.

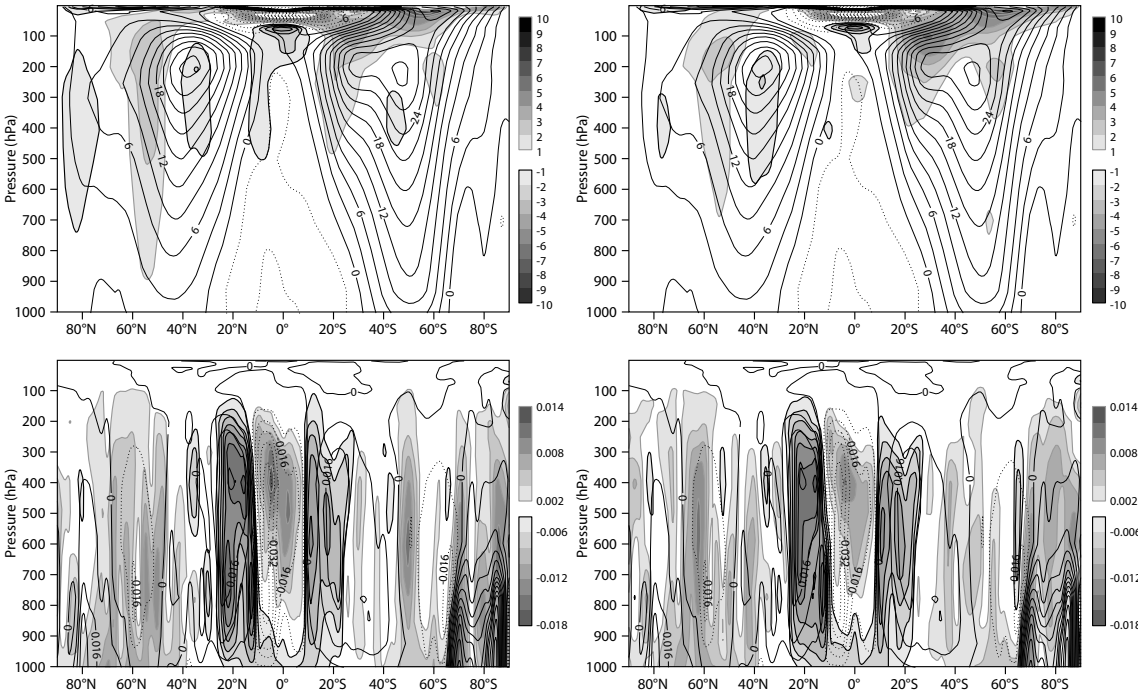

FIG. 8. As in Fig. 7, but for the zonal wind (top panels, in $m\ s^{-1}$) and vertical velocity (bottom panels, in $Pa\ s^{-1}$). Left column is for the operational model; right one for the model with McRad.

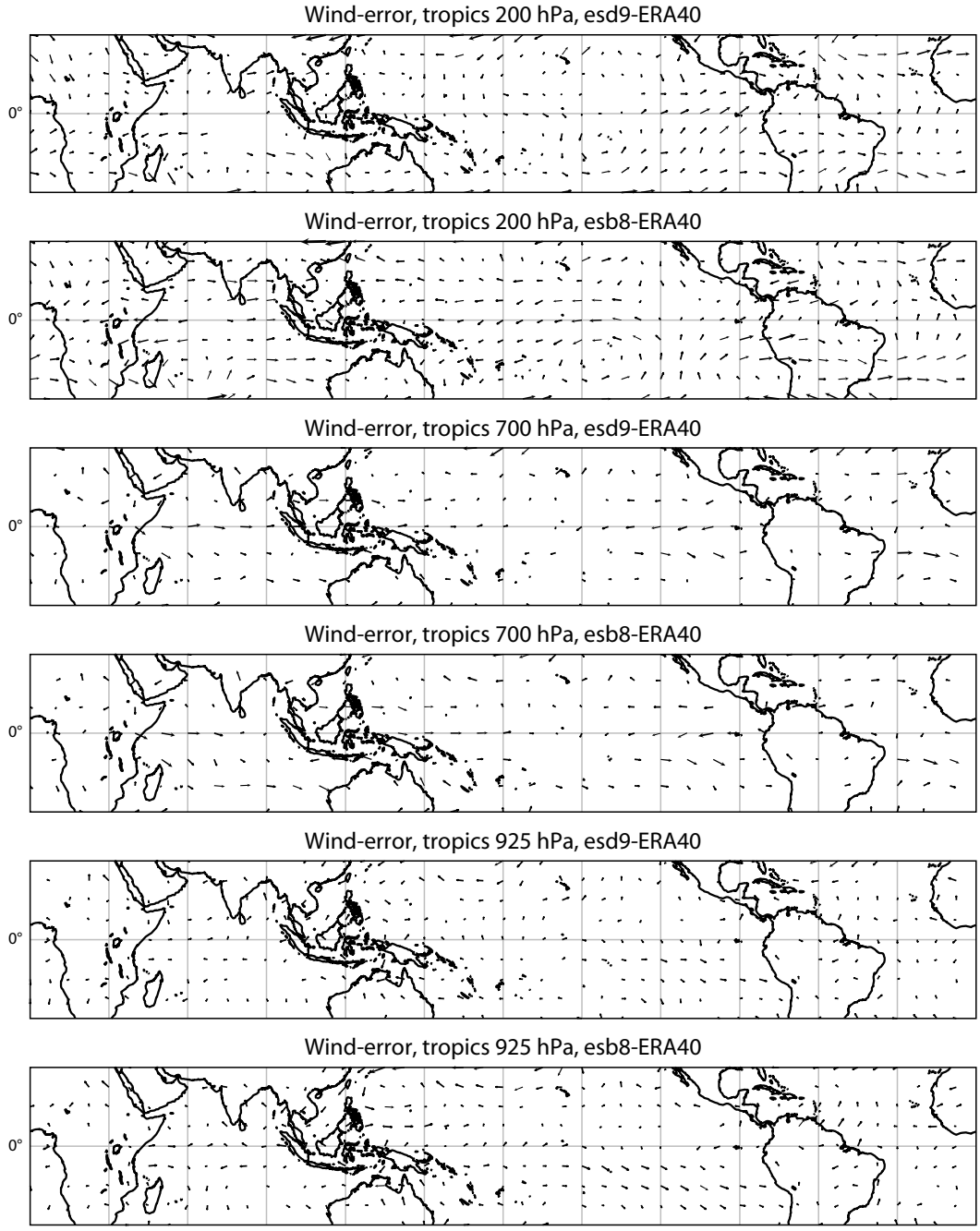

FIG. 9. The difference in wind between the annual averages from model simulations and ERA40. Top two panels for 200 hPa, middle two for 700 hPa, bottom two panels for 925 hPa. For each pair, the upper panel is the McRad model, the lower with OPE.

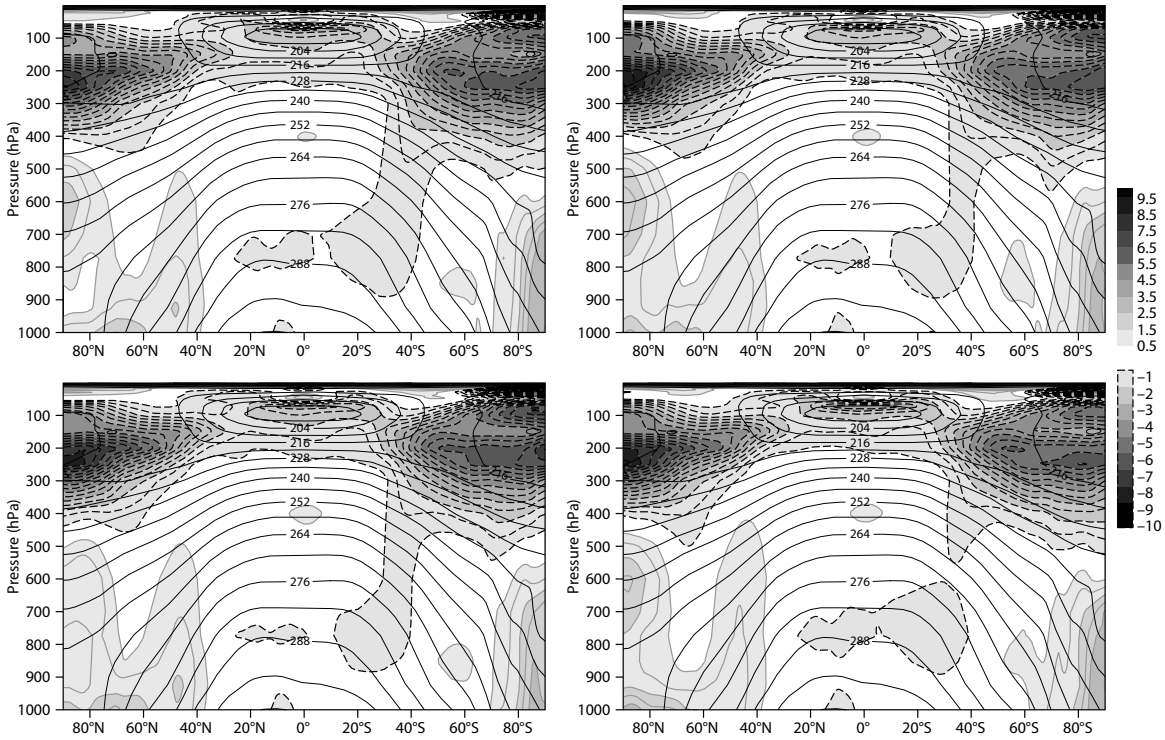

FIG. 10. The difference with ERA40 analysis for temperature (top panels, in K). Top left is the McRad model with generalized overlap of cloud layers with a decorrelation length for cloud cover DLCC=2 km and and a decorrelation length for cloud water DLCW=1 km, top right with DLCC=4 km and DLCW=2 km, bottom left with DLCC=5 km and DLCW=1 km. Bottom right is the McRad model with maximum-random overlap of homogeneous clouds.

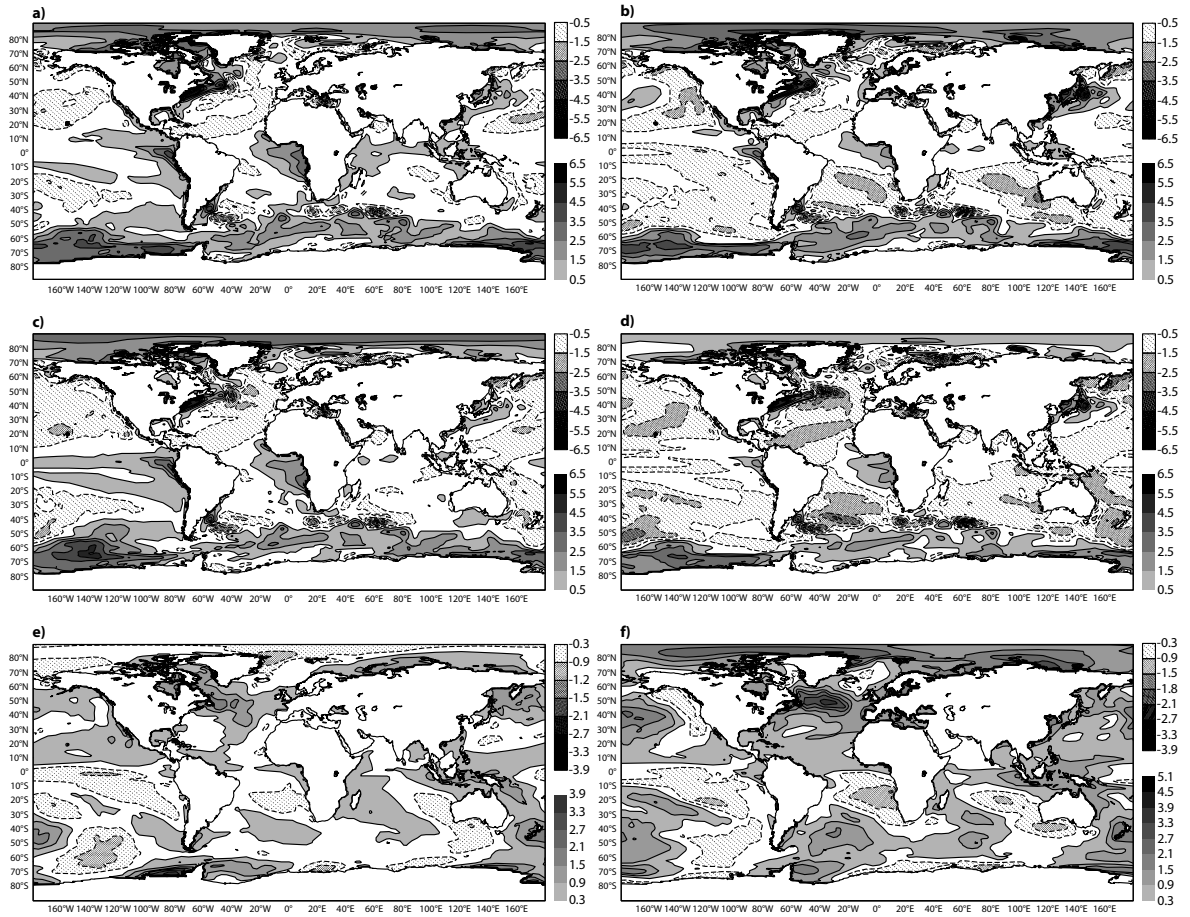

FIG. 11. Comparison of annual mean sea surface temperature (SST) produced by the $T_L159R63$ model for year 1 (left panels) and year 2 (right panels). Top panels are the differences between the McRad 32R2 model and ERA40 SSTs, middle panels the differences between the OPE model and ERA40 SSTs, lower panels are the differences between the McRad and OPE models. All values in K.

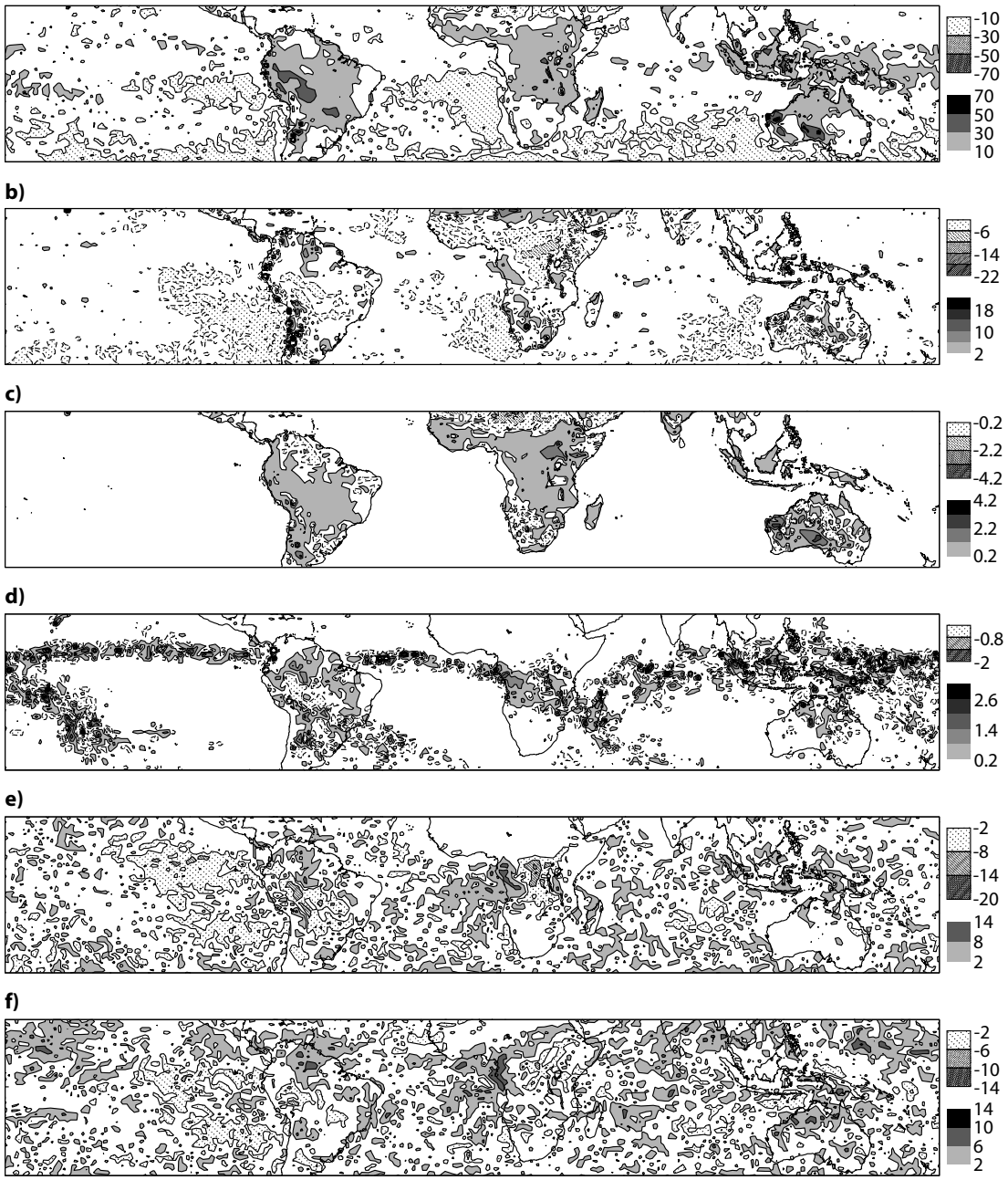

FIG. 12. Differences in surface parameters ($\Delta x = McRad - 31R2$) between the McRad and the 31R2 model for the month of January 2007. From top to bottom, are the differences in (a) net solar radiation at the surface (Wm^{-2}), (b) net long-wave radiation at the surface (Wm^{-2}), (c) surface temperature (K), (d) total precipitation ($mm\ day^{-1}$), (e) low-level cloudiness ($percent$) and (f) total cloudiness ($percent$). All quantities are averaged over the 62 12-hour forecasts starting at 00 and 12 GMT over the month of January 2007.

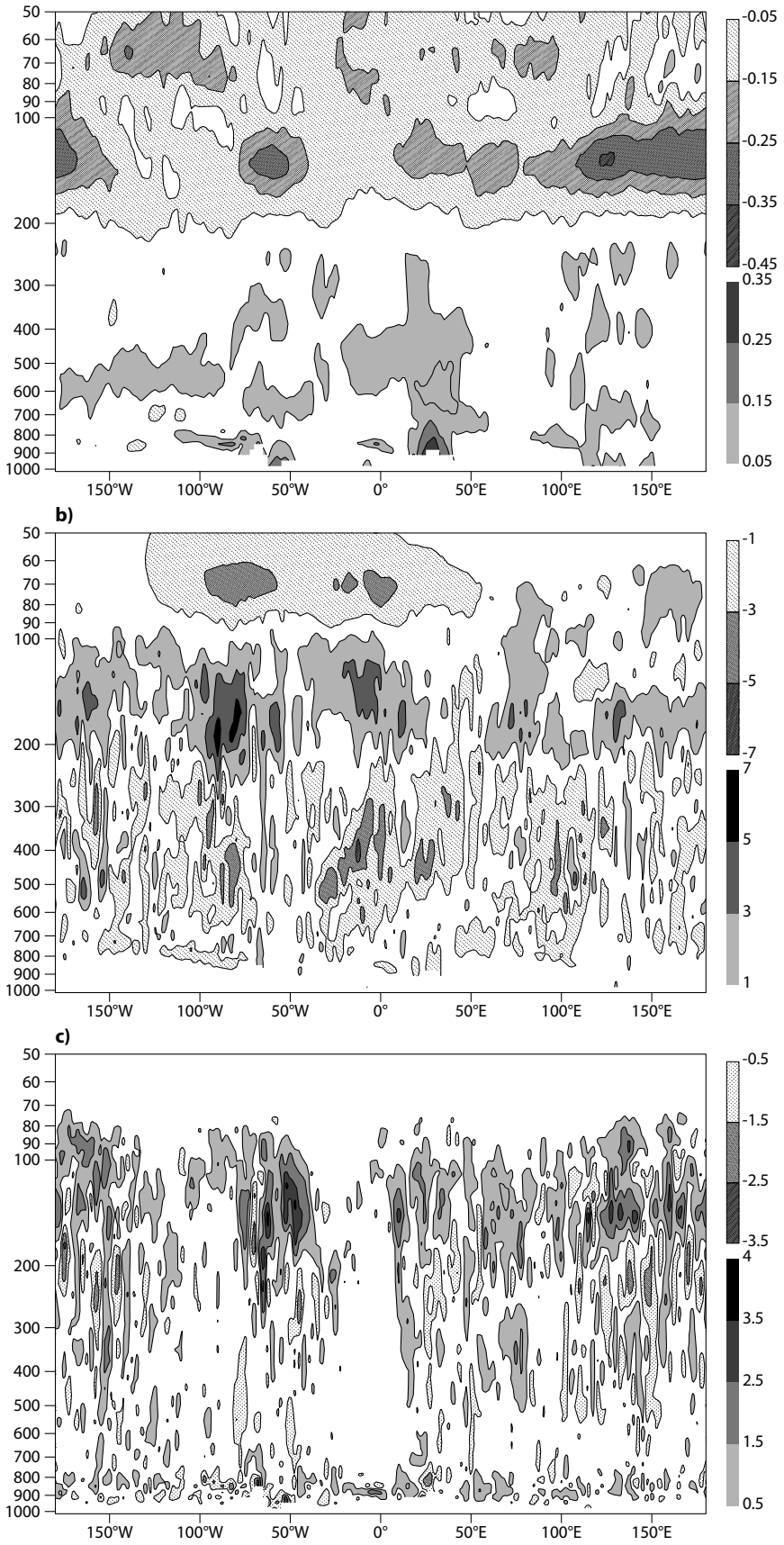

FIG. 13. As in Fig. 12, but for the differences in atmospheric parameters Δx averaged over the 10^oN - 30^oS latitude band. Top panel is for temperature (ΔT with steps of 0.1 K from +/- 0.05 K), middle panel for specific humidity ($\Delta Q/Q$ with steps of 2 $percent$ from +/- 1 $percent$), bottom panel for cloud cover (ΔCC with steps of 1 $percent$ from +/- 0.5 $percent$).

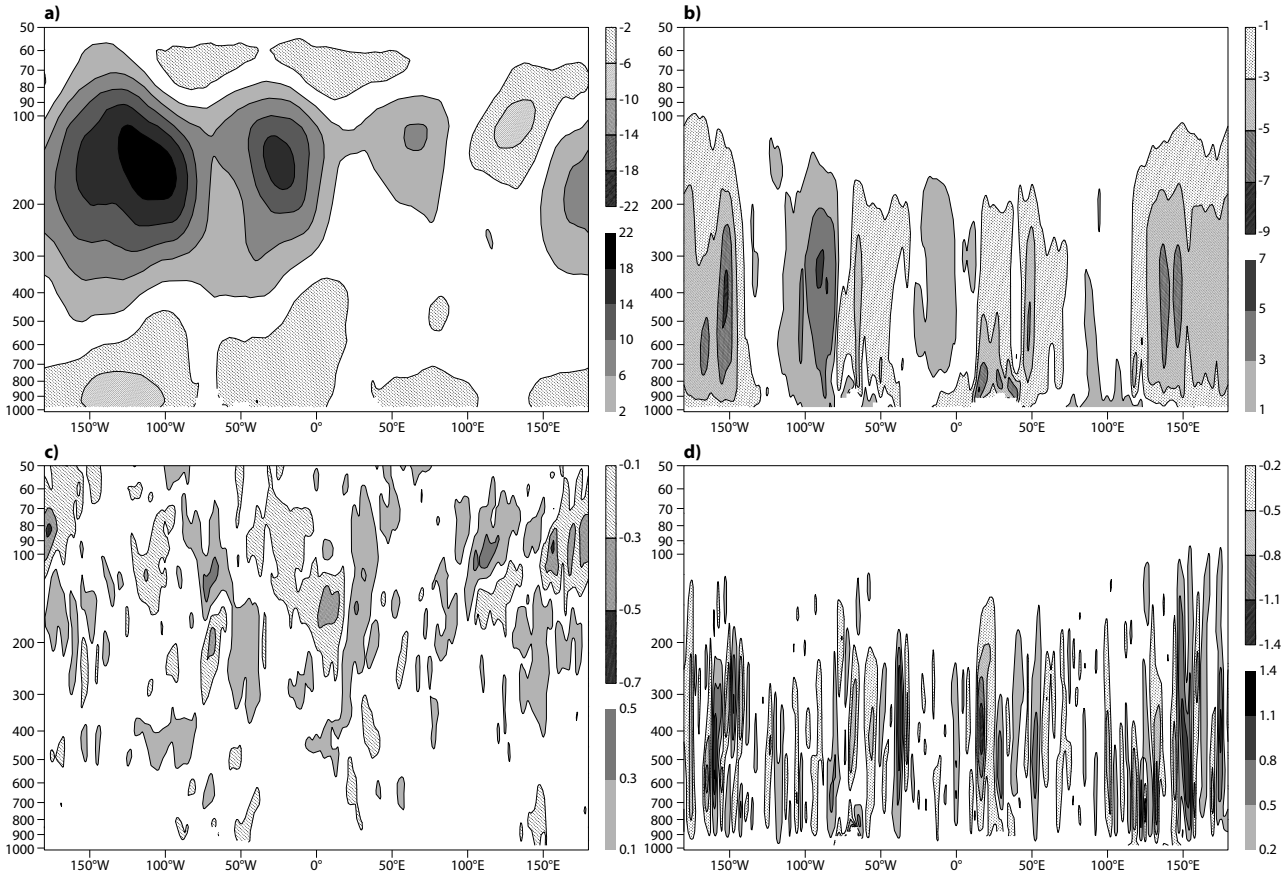

FIG. 14. Atmospheric parameters in the McRad and the 31R2 model for the month of January 2007 in same conditions as in Fig. 12. Top panels are for McRad, middle panels for 31R2, bottom panels are the differences McRad - 31R2. Left column is for the zonal wind (steps of 3 $m\ s^{-1}$ from -3 $m\ s^{-1}$ for easterlies, steps of 5 $m\ s^{-1}$ from 5 $m\ s^{-1}$ for westerlies. Right column is for the vertical velocity (steps of 0.02 $Pa\ s^{-1}$ from +/- 0.01 $Pa\ s^{-1}$). In bottom panels, steps are of 0.2 $m\ s^{-1}$ from +/- 0.1 $m\ s^{-1}$ for ΔU, and of 0.04 $unit$ from +/- 0.02 $unit$ for ΔW (Note that for this last panel $unit$ is $10^{-1} Pa\ s^{-1}$.

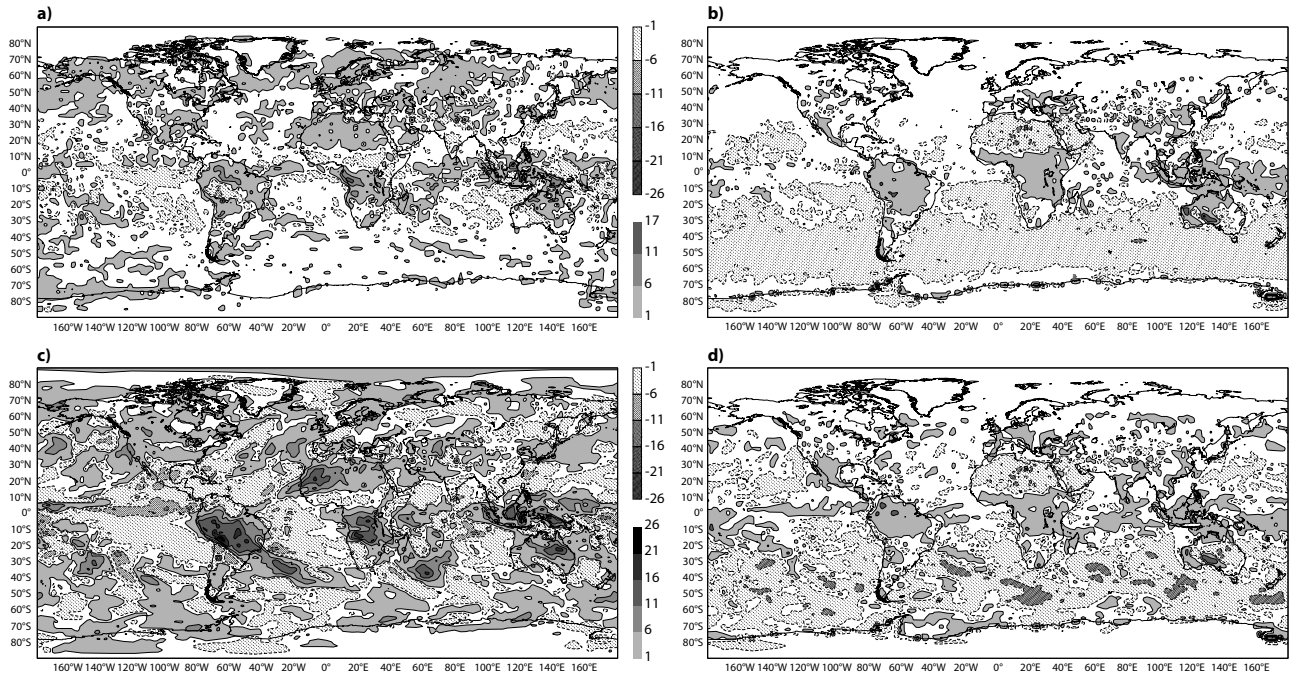

FIG. 15. The difference in outgoing long-wave radiation (left) and absorbed short-wave radiation (right) at the top of the atmosphere between the McRad and the 31R2 model for the month of January 2007. Upper panel is the average over the first 24 hours, lower panel over the last 24 hours of the ten-day forecasts. All quantities in $W\ m^{-2}$.

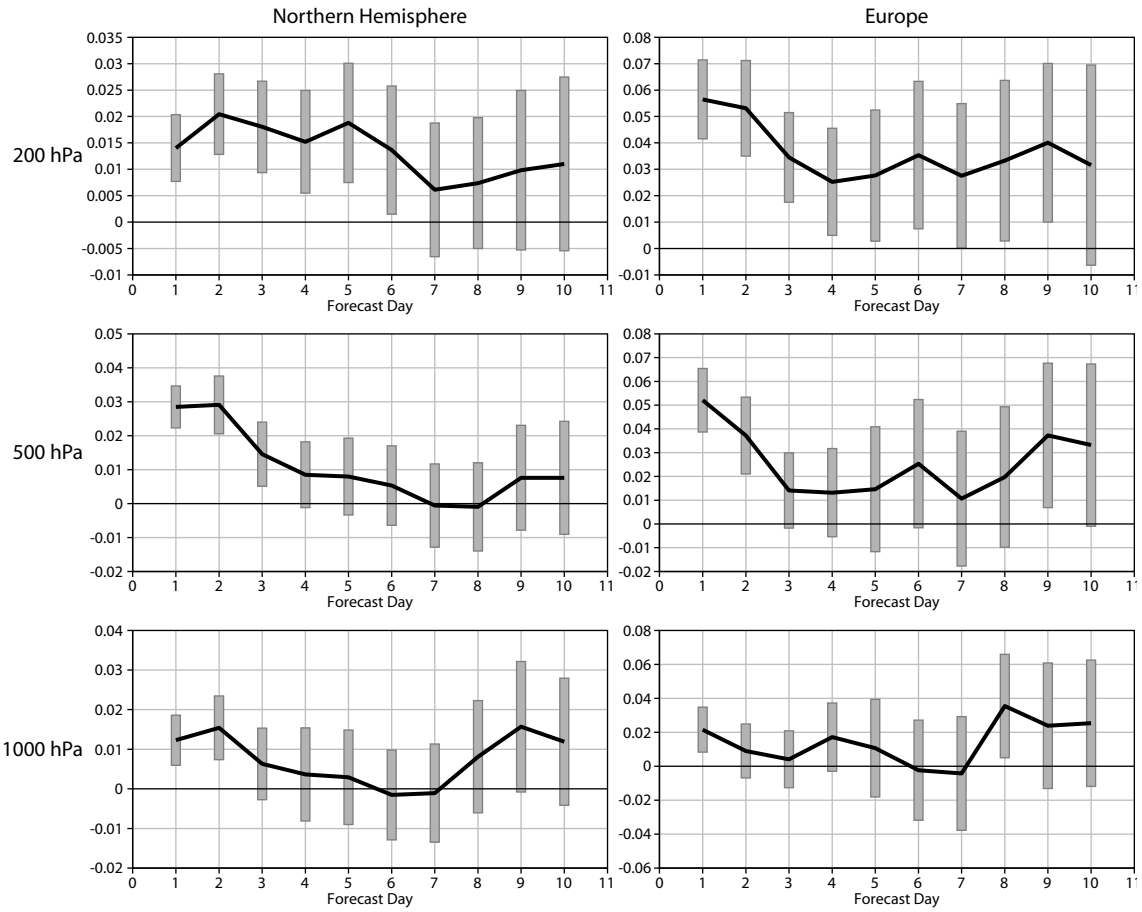

FIG. 16. The time-series of the difference in r.m.s. error on the geopotential in the Northern hemisphere (left column), European area (middle column) and Southern hemisphere (right column) at 200, 500 and 1000 hPa (from top to bottom panels) over the period 20061201-20070430. Unit is $m^2\ s^{-2}$. A value above the zero line denotes an improvement of the McRad forecasts with respect to the operational forecasts.

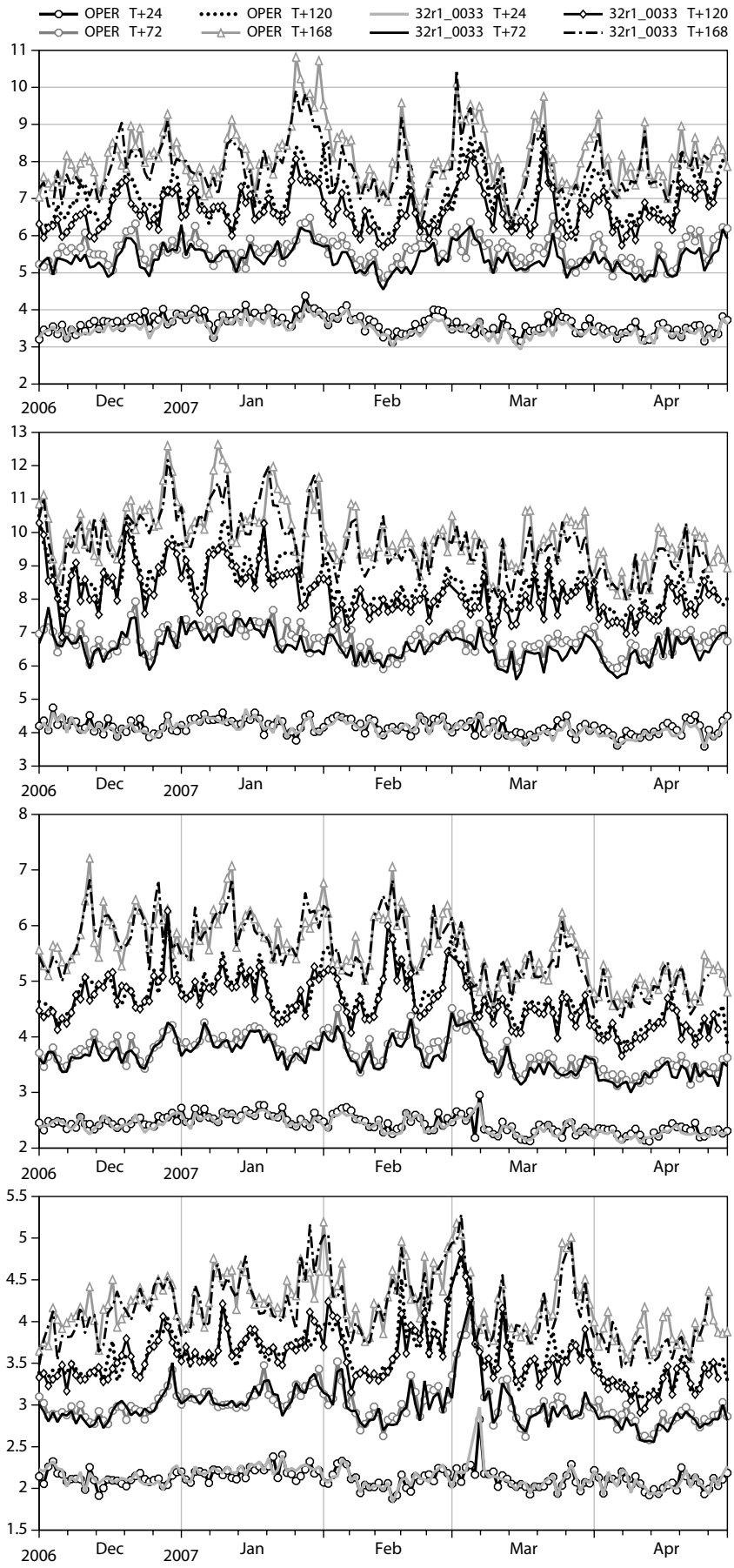

FIG. 17. The time-series of the r.m.s. error on the vector wind in the Tropics ($20^oN - 20^oS$) at 100, 200, 500 and 850 hPa (from top to bottom panels) over the period 20061201-20070430.

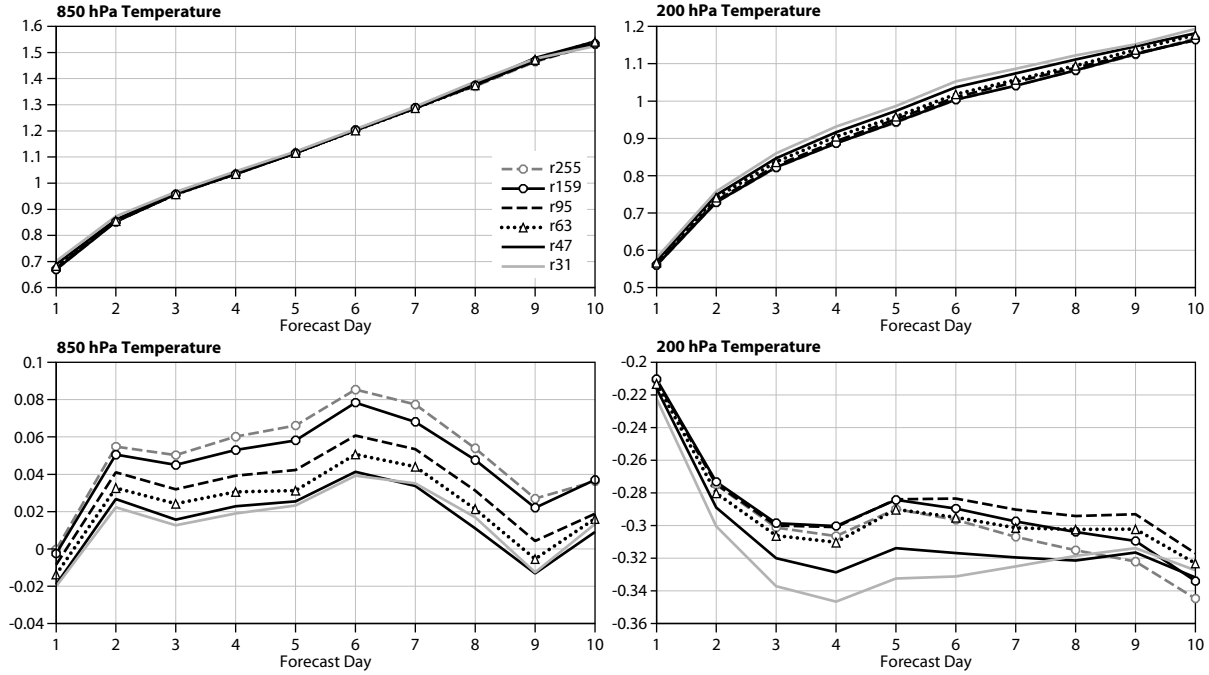

FIG. 18. The r.m.s. error (top panels) and mean error (bottom panels) of the temperature at 850 hPa (left panels) and 200 hPa (right panels) for McRad 10-day forecasts at $T_L399L62$, started every 96 hours from 2006021212 to 2007020512, and using the six different radiation grids from $R255$ to $R31$ given in Table 4.

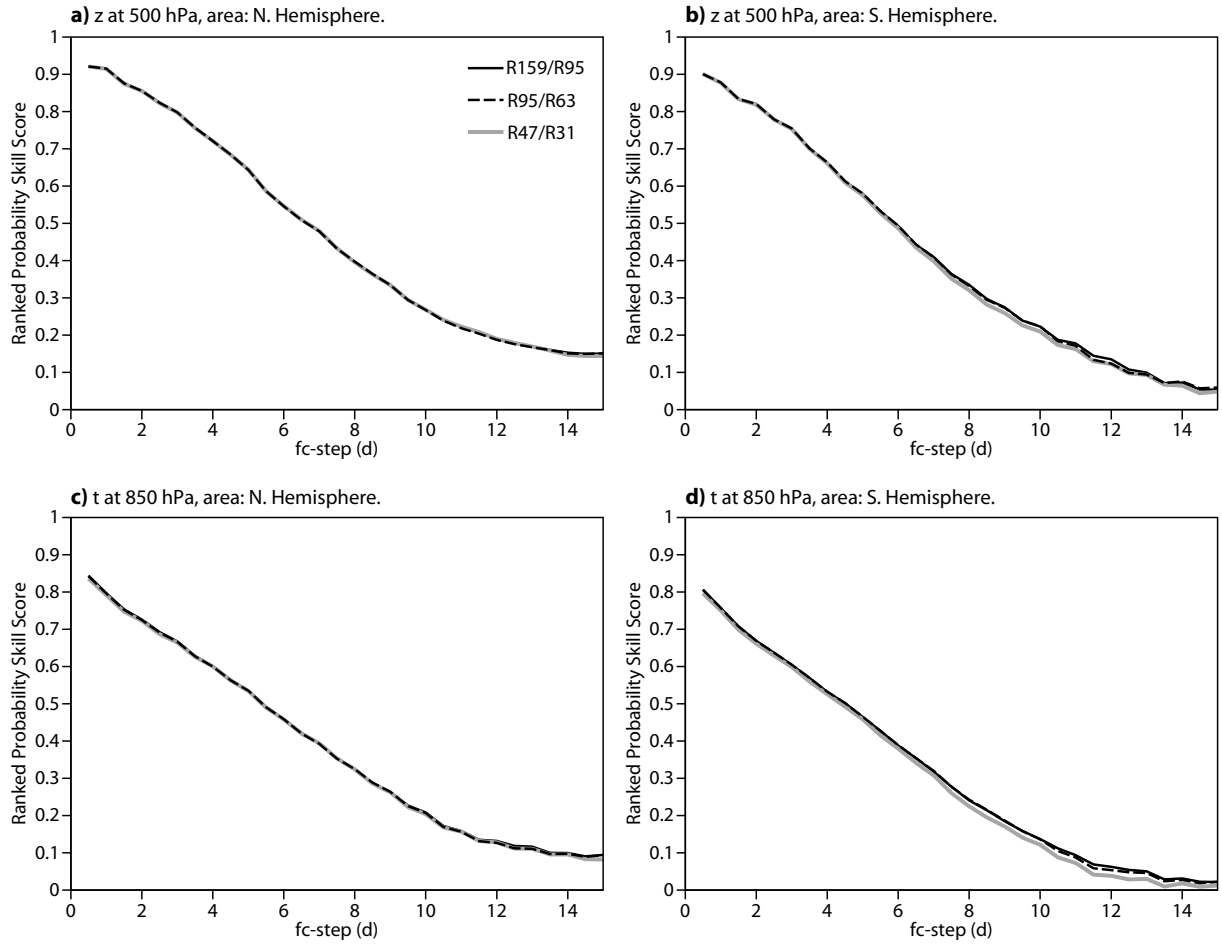

FIG. 19. The ranked probability skill score for the geopotential at 500 hPa (upper panels) and the temperature at 850 hPa (lower panels) for the Northern (left column) and Southern (right column) hemispheres for the 32R2 EPS, with three sets of radiation grids: Black curve is for R159/R95, red for R95/R63, blue for R47/31.